Polyunsaturated fatty acid analogues differentially affect cardiac Na_v, Ca_v, and K_v channels through unique mechanisms

Briana M. Bohannon[1], Xiaoan Wu[1], Marta E. Perez[1], Sara I. Liin[2] and H. Peter Larsson[1]

[1]Department of Physiology and Biophysics, Miller School of Medicine, University of Miami, Miami, FL 33136, USA.

[2]Department of Clinical and Experimental Medicine, Linköping University. SE-581 85 Linköping, Sweden.

Corresponding authors:

H. Peter Larsson

Department of Physiology and Biophysics,
Miller School of Medicine,
University of Miami,
1600 NW 10th Avenue,
Miami, FL 33136, USA.

plarsson@med.miami.edu, ph: 305-243-1021

Key words: I_{Ks}, Cav1.2, Nav1.5, Long QT Syndrome, polyunsaturated fatty acids

Abstract

The cardiac ventricular action potential depends on several voltage-gated ion channels, including Na_v, Ca_v, and K_v channels. Mutations in these channels can cause Long QT Syndrome (LQTS) which increases the risk for ventricular fibrillation and sudden cardiac death. Polyunsaturated fatty acids (PUFAs) have emerged as potential therapeutics for LQTS because they are modulators of voltage-gated ion channels. Here we demonstrate that PUFA analogues vary in their selectivity for human voltage-gated ion channels involved in the ventricular action potential. The effects of specific PUFA analogues range from selective for a specific ion channel to broadly modulating all three cardiac ion channels (N_{aV}, C_{aL}, and I_{Ks}). In addition, PUFA analogues do not modulate these channels through a shared mechanism. Our data suggest that different PUFA analogues could be tailored towards specific forms of LQTS, which are caused by mutations in distinct cardiac ion channels, and thus restore a normal ventricular action potential.

Introduction

The ventricular action potential is mediated by the coordinated activity of several different voltage-dependent ion channels (1). The rapid upstroke of the ventricular action potential is mediated by the activation of the voltage-gated Na^+ channel, Nav1.5, which then rapidly inactivates. The activation of L-type voltage gated Ca^{2+} channels, Cav1.2, and influx of Ca^{2+} leads to a sustained depolarization, or plateau phase, and the contraction of the cardiac muscle. Inactivation of Cav1.2 channels along with the activation of the slow delayed-rectifier K^+ channels, Kv11.1 (which generates the I_{Kr} current) and Kv7.1/KCNE1 (which generates the I_{Ks} current), work to promote repolarization of the cell membrane (2). Mutations of any of these ion channels (or channelopathies) could lead to Long QT Syndrome (LQTS), which is an arrhythmogenic disorder that predisposes the individual to potentially fatal cardiac arrhythmias (3, 4).

The Nav1.5 α-subunit contains four non-identical linked domains, DI-DIV. Each of these domains contain 6 transmembrane segments (S1-S6), where the S1-S4 segments make up the voltage-sensing domains (VSD) and S5-S6 segments make up the pore domains (PD). The S4 helix of each of the four domains contains a motif with positively charged amino acid residues which allow the S4 segment to detect and respond to changes in the membrane electric field, acting as the channel voltage sensor (5). The movement of these voltage sensors determines the voltage dependence of activation and inactivation, where activation of the DI-III S4s are suggested to promote activation and activation of DIV S4 segment is sufficient to induce voltage-dependent inactivation of Nav1.5 (6). The Nav1.5 α-subunit exists as a macromolecular complex with the accessory subunit β1. β1 is a single transmembrane spanning helix that modifies the

kinetics of Nav1.5 channel activation and inactivation and can alter the pharmacology of the Nav1.5 α-subunit (7-9). Gain-of-function mutations of Nav1.5 increase Na^+ currents and lead to LQTS Type 3 (LQT3) (10-12).

Like Nav1.5, the Cav1.2 α-subunit contains four linked domains, DI-DIV, where each domain consists of 6 transmembrane segments S1-S6. S1-S4 form the VSD, where S4 acts as the voltage sensor, and S5-S6 form the PD. Cav1.2 exists as a large macromolecular complex with the accessory subunits β3 and α2δ subunits that are important for membrane expression and alter channel activation and deactivation kinetics, respectively (13, 14). Cav1.2 undergoes both voltage-dependent inactivation and calcium-dependent inactivation (15, 16) which allows it to regulate Ca^{2+} influx into the cardiomyocyte. Gain-of-function mutations of Cav1.2 increase Ca^{2+} currents and lead to Long QT Type 8 (LQT8) (17, 18).

The voltage-gated K^+ channel, Kv7.1, along with the auxiliary subunit KCNE1, mediates an important repolarizing K^+ current, I_{Ks} (19-21). The Kv7.1 α-subunit contains 6 transmembrane segments, S1-S6. S1-S4 comprise the VSD, where S4 contains several positively charged amino acid residues that allow S4 to act as the voltage sensor of Kv7.1. S5-S6 segments comprise the channel PD. Kv7.1 forms a tetrameric channel, where 4 Kv7.1 α-subunits arrange to form a functional channel. The auxiliary β-subunit KCNE1 drastically modulates Kv7.1 channel voltage dependence, activation kinetics, and single-channel conductance (22, 23). Loss-of-function mutations in the Kv7.1 α-subunit and KCNE1 β-subunit lead to reductions in I_{Ks} and can lead to LQTS Type 1 (LQT1) and Type 5 (LQT5) (24-28), respectively.

Polyunsaturated fatty acids (PUFAs) are amphipathic molecules that have been suggested to possess antiarrhythmic effects (29, 30). PUFAs are characterized by having a long hydrocarbon tail with two or more double bonds, as well as having a charged, hydrophilic head group (31). PUFAs, such as DHA and EPA, have been shown to prevent cardiac arrhythmias in animal models and cultured cardiomyocytes by inhibiting the activity of Na_v and Ca_v channels (30, 32-34). Specifically, DHA and EPA are thought to bind to discrete sites on the channel protein to stabilize the inactivated states of the Nav and Cav channels (32, 35). Since the voltage sensors of Nav and Cav channels are relatively homologous, it has been suggested that PUFAs act on the voltage-sensing S4 segments that control inactivation in these channels (30, 32). Our group has demonstrated that PUFAs and PUFA analogues also modulate the activity of the Kv7.1/KCNE1 channel and work to promote voltage-dependent activation of the I_{Ks} current (36-38). The mechanism through which PUFAs promote Kv7.1/KCNE1 activation is referred to as the lipoelectric hypothesis which involves the following: 1) the PUFA molecule integrates into the membrane via its hydrocarbon tail and 2) the negatively charged PUFA head group electrostatically attracts the positively charged S4 segment and facilitates the outward movement of S4, promoting I_{Ks} channel activation (36). Our group has also demonstrated that PUFAs and modified PUFAs exert a second effect on the pore of Kv7.1 through an additional electrostatic interaction with a lysine residue (K326) in the S6 segment (39). This electrostatic interaction between the negatively charged PUFA head group and K326 leads to an increase in maximal conductance of the channel (G_{max}) (39).

Some groups have suggested that PUFAs could modify Na_v channels by causing a leftward shift in voltage dependent inactivation through an electrostatic effect on the voltage-sensing domains involved in inactivation (30, 32). It is possible that PUFAs modulate Kv7.1/KCNE1, Nav, and Cav channels by a similar mechanism by integrating next to the S4 voltage sensors and electrostatically attracting the voltage sensors toward their outward position. If PUFAs integrate preferentially next to the S4 that controls inactivation in Nav and Cav channels but next to all S4s in Kv7.1/KCNE1 channels, PUFAs would promote activation in Kv7.1/KCNE1 channels but promote inactivation in Nav and Cav channels. Though both PUFAs and PUFA analogues are known to modulate different ion channel activities (i.e. processes underlying activation and inactivation), it is unclear whether specific PUFAs and PUFA analogues are selective for certain ion channels or if they broadly influence the activity of several different ion channels simultaneously.

In this work, we characterize the channel-specific effects of different PUFAs and PUFA analogues in order to further understand which PUFAs and PUFA analogues would be the most therapeutically relevant in the treatment for different LQTS subtypes. We have found that PUFA analogues modulate Kv7.1/KCNE1, Cav1.2, and Nav1.5 through different mechanisms instead of through a shared mechanism. In addition, we demonstrate that PUFA analogues exhibit a broad range of differences in selectivity for Kv7.1/KCNE1, Cav1.2, and Nav1.5. Lastly, PUFA analogues that are more selective for Kv7.1/KCNE1 are able restore a prolonged ventricular action potential and prevent arrhythmia in simulated cardiomyocytes.

Results

PUFA analogues modulate Kv7.1/KCNE1, Cav1.2, and Nav1.5 through distinct mechanisms.

There are several studies supporting electrostatic activation of Kv7.1/KCNE1 channels by PUFA analogues (37-39, 41). PUFAs are known to inhibit Na_v and Ca_v channels, but there is little evidence on the mechanism of channel inhibition using a diverse set of PUFA analogues. Previous groups have suggested that PUFAs may inhibit Na_v and Ca_v channels by interacting with S4 voltage sensors and stabilizing the inactivated state since there are similarities between the voltage sensor profiles of Na_v and Ca_v channels. (30, 32-34). For this reason, we hypothesize that PUFA analogues inhibit Cav1.2 and Nav1.5 through a shared electrostatic mechanism on S4 voltage sensors, similar to that reported with Kv7.1/KCNE1 channels. But in the case of Na_v and Ca_v channels, PUFAs would left-shift the voltage dependence of inactivation instead of activation which is seen in Kv7.1/KCNE1. To compare the effects of different PUFA analogues on these three different channels, we here measure the currents from Kv7.1/KCNE1, Cav1.2, and Nav1.5 expressed in *Xenopus* oocytes using two-electrode voltage clamp.

We first illustrate the effects of a representative PUFA analogue Linoleoyl taurine (Lin-taurine) on the voltage dependence of activation and the conductance of Kv7.1/KCNE1 (Fig. 1A-C). These effects are reflected in the tail current-voltage relationship where the effects on the voltage sensor are measured as a leftward shift in the voltage dependence of activation and the effects on the conductance are measured as a relative increase in the maximal conductance upon PUFA application (Fig. 1C). We also measure the effect of Lin-taurine on Cav1.2 and Nav1.5 channels (Figure 2-3). When we apply Lin-taurine to the Cav1.2 macromolecular complex (Fig. 2A), we see that Lin-taurine reduces Ca^{2+} currents in a dose-dependent manner (Fig. 2B-C). However, Lin-taurine reduces Ca^{2+} current without shifting the voltage-dependence of Cav1.2 activation (Fig. 2B-C; Supplemental Fig. 1). We use a depolarizing pre-pulse protocol to measure changes in voltage-dependent inactivation (Fig. 2D-E). When we measure the effects of PUFA analogues on voltage-dependent inactivation, we see again a decrease in Ca^{2+} currents, but surprisingly no shift in voltage-dependent inactivation (Fig. 2D-E). This suggests that PUFA analogues do not inhibit Cav1.2 channels through a shared electrostatic mechanism on S4 voltage sensors that shifts the voltage dependence of S4 movement, but rather through a mechanism that reduces either the number of conducting channels (potentially through an effect on the pore) or the maximum conductance of each channel. When we apply Lin-taurine to Nav1.5 (Figure 3A) and measure voltage-dependent activation, we see a dose-dependent inhibition of Na^{+} currents with no shift in the voltage dependence of activation (Fig. 3B-C; Supplemental Fig. 1). However, when we measured voltage-dependent inactivation of Nav1.5, we observed that PUFA analogues left-shift the voltage dependence of inactivation (Fig.

168 3D-E). In addition to the left-shift in voltage-dependent inactivation, we also observe a
169 dose-dependent decrease in Nav1.5 currents (Fig. 3E). This suggests that PUFA
170 analogues, while they do influence the voltage dependence of inactivation, may also
171 have an additional effect on the conductance of Nav1.5, leading to the dose-dependent
172 decrease in Na^+ currents seen on top of the leftward shift of the voltage dependence of
173 inactivation.
174
175 Through these data, we observe that PUFA analogues modulate cardiac voltage-gated
176 ion channels through non-identical mechanisms. PUFA analogues promote the
177 activation of Kv7.1/KCNE1 through electrostatic effects that left-shift the voltage
178 dependence of activation and an increase in the maximal conductance. PUFA
179 analogues inhibit Cav1.2 channels through an apparent effect on the pore leading to a
180 reduction in Ca^{2+} current but without producing any leftward shift in the voltage
181 dependence of inactivation. In addition, PUFA analogues inhibit Nav1.5 through a
182 combination of a leftward shift in the voltage dependence of inactivation and an effect
183 on the maximum conductance, which leads to a dose-dependent decrease in Na^+
184 current. Together these findings show that PUFA analogues affect Kv7.1/KCNE1,
185 Nav1.5, and Cav1.2 channels through different mechanisms.
186
187

188 *PUFA analogues with taurine head groups are non-selective and broadly modulate*
189 *multiple cardiac ion channels, with preference for Cav1.2 and Nav1.5.*
190 We have found through previous work that PUFA analogues with taurine head groups
191 are good activators of the Kv7.1/KCNE1 channels due to the low pKa of the taurine
192 head group (37, 38). Having a lower pKa allows the taurine head group to be fully
193 negatively charged at physiological pH so that it has maximal electrostatic effects on
194 Kv7.1/KCNE1 channels (38). We tested a set of PUFA analogues with taurine head
195 groups on Kv7.1/KCNE1, Cav1.2, and Nav1.5 channels to determine if these effects are
196 selective for the Kv7.1/KCNE1 channel or if taurine analogues also modulate Cav1.2
197 and Nav1.5 channels. Lin-taurine is a PUFA analogue with a taurine head group (Figure
198 4A) that promotes the activation of the cardiac Kv7.1/KCNE1 channel, by promoting a
199 leftward shift in the voltage-dependence of activation by -39.9 ± 3.6 mV at 7 μM ($p = 0.008$) (Fig 4B). In addition, the application of Lin-taurine produces a slight, but not
200
201 statistically significant increase in the maximal conductance of the Kv7.1/KCNE1
202 channel at 7 μM (1.9 ± 0.6; $p = 0.26$) (Fig. 4C). Lin-taurine inhibits Cav1.2 current in a
203 dose-dependent manner without left-shifting the voltage dependence of inactivation for
204 Cav1.2 (2.8 ± 1.4 mV; $p = 0.17$), but instead by significantly decreasing the G_{max} at 7 μM
205 (0.4 ± 0.1; $p = 0.03$) (Fig. 4D-E). Lastly, Lin-taurine inhibits Nav1.5 current by left-
206 shifting the voltage dependence of inactivation (-23.5 ± 1.9 mV; $p = 0.001$) and also
207 decreasing the G_{max} at 7 μM (0.5 ± 0.07; $p = 0.005$) (Fig 4F-G).
208
209 N-arachidonoyl taurine (N-AT) is a PUFA analogue with a taurine head group that has
210 been demonstrated by our group to promote activation of Kv7.1/KCNE1, left-shifting the

voltage-dependence and increasing the G_{max} at 70 μM (Fig. 5A) (38). Here, we used lower concentrations (0.2, 0.7, 2, 7, and 20 μM) with the goal of understanding the selectivity of N-AT for cardiac ion channels and at more therapeutically feasible concentrations. Application of N-AT does not promote activation of Kv7.1/KCNE1 in this lower concentration range, does not left-shift of the voltage-dependence of activation (-1.8 ± 2.6 mV; p = 0.5), and does not increase the G_{max} at 7 μM (0.9 ± 0.03; p = 0.98) (Fig. 5B-D). However, N-AT causes a dose-dependent decrease in Cav1.2 current, though does not cause a significant shift in the voltage dependence of inactivation (13.5 ± 3.8 mV; p = 0.07), nor does it cause a significant reduction in the overall G_{max} (0.6 ± 0.1; p = 0.06) at 7 μM (Fig. 5E-G). In addition, N-AT decreases Nav1.5 current, produces a leftward shift in voltage-dependent inactivation (-16.7 ± 3.5 mV; p = 0.04), and significantly reduces the G_{max} at 7 μM (0.3 ± 0.04; p = 0.004) (Fig. 5H-J). This data suggests that N-AT is more selective for Cav1.2 and Nav1.5, compared to Kv7.1/KCNE1.

Pinoleoyl taurine (Pin-taurine) promotes the activation of Kv7.1/KCNE1 in a dose-dependent manner (Fig. 6A-B). Pin-taurine, like Lin-taurine, promotes a leftward shift in the voltage dependence of activation (-23.8 ± 2.7 mV; p = 0.003) and increases the G-$_{max}$ of Kv7.1/KCNE1 at 7 μM with a trend towards significance (2.2 ± 0.4; p = 0.06) (Fig. 6C-D). Pin-taurine also inhibits Cav1.2 current, but does not significantly shift the voltage-dependence of inactivation (4.1 ± 2.2 mV; p = 0.13) and does not significantly decrease the G_{max} at 7 μM (0.8 ± 0.1; p = 0.2) (Fig. 6E-G). Pin-taurine inhibits Nav1.5 currents and does so by significantly left-shifting the voltage dependence of inactivation

(-16 ± 2.7 mV; p = 0.01) and decreasing the G_{max} at 7 μM (0.4 ± 0.09; p = 0.005) (Fig. 6H-J).

DHA-taurine promotes the activation of Kv7.1/KCNE1 channels in a dose-dependent manner, left-shifting the voltage-dependence of activation (-45.3 ± 2.9 mV; p = 0.004) and significantly increasing the G_{max} at 7 μM (1.7 ± 0.1; p = 0.03) (Fig. 7A-C). DHA-taurine application results in dose-dependent inhibition of Cav1.2 current (Fig. 7E), but does not significantly left-shift the voltage-dependence of inactivation at 7 μM (0.2 ± 0.8 mV; p = 0.85) (Fig. 7F). Instead, DHA-taurine causes a significant decrease in the G_{max} of Cav1.2 at 7 μM (0.4 ± 0.01; p < 0.001) (Fig. 7G). Lastly, DHA-taurine inhibits Nav1.5 by inducing a significant left-shift in the voltage-dependence of inactivation (-28.5 ± 0.6 mV; p < 0.001) and decreasing the G_{max} at 7 μM (0.05 ± 0.01; p < 0.001) (Fig. 7H-I). These results suggest that PUFA analogues with taurine head groups exhibit broad selectivity for multiple ion channels.

PUFA analogues with glycine head groups tend to be more selective for Kv7.1/KCNE1 with lower affinity for Cav1.2 and Nav1.5.

PUFA analogues with glycine head groups have also been shown to effectively activate the Kv7.1/KCNE1 channel (37). The glycine head group has a lower pKa than regular PUFAs with a carboxyl head group (37), thereby allowing the head group to be more deprotonated and partially negatively charged at physiological pH. For this reason, PUFA analogues with glycine head groups are able to electrostatically activate Kv7.1/KCNE1 channels (37). We here tested several glycine compounds on

Kv7.1/KCNE1, Cav1.2, and Nav1.5 channels to determine whether they have selective or non-selective effects on cardiac ion channels.

We first examined Linoleoyl glycine (Lin-glycine). Lin-glycine promotes the activation of the cardiac Kv7.1/KCNE1 channel by left-shifting the voltage dependence of channel activation to more negative voltages at 7 μM (-23.8 ± 1.6 mV; $p < 0.001$). Application of Lin-glycine also increases the G_{max} of Kv7.1/KCNE1 at 7 μM (2.3 ± 0.2; $p = 0.008$) (Fig. 8A-D). Lin-glycine inhibits Cav1.2 in a dose-dependent manner (Fig. 8E), but does not left shift the voltage dependence of inactivation (0.6 ± 2.3 mV; $p = 0.65$). Instead, Lin-glycine produces a decrease of the G_{max} at 7 μM, but this decrease is not statistically significant (0.3 ± 0.2; $p = 0.07$) (Fig. 8F-G). Lin-glycine causes a dose-dependent decrease of Nav1.5 current, left-shifts the voltage dependence of inactivation (-15.2 ± 2.8 mV; $p = 0.01$), and reduces the G_{max} at 7 μM (0.5 ± 0.1; $p = 0.007$) (Fig. 8H-J).

Pinoleoyl glycine (Pin-glycine) promotes the activation of Kv7.1/KCNE1 channels in a dose-dependent manner (Fig. 9A-B). Pin-glycine induces a left-shift in the voltage-dependence of activation (-8.7 ± 1.8 mV; $p = 0.04$) and increases the G_{max} at 7 μM (1.7 ± 0.1; $p = 0.03$) (Fig. 9C-D). Pin-glycine, however causes little inhibition of Cav1.2 current (Fig. 9E). Pin-glycine produces no shift in the voltage dependence of inactivation (-3.1 ± 4.2 mV; $p = 0.54$) and does not significantly reduce the G_{max} of Cav1.2 channels at 7 μM (0.8 ± 0.1; $p = 0.34$) (Fig. 9F-G). Pin-glycine inhibits Nav1.5 channels in a dose-dependent manner, but does not produce a significant left-shift in the voltage

dependence of inactivation at 7 μM (-4.7 ± 1.9 mV; p = 0.09). However, there is a statistically significant reduction in the G_{max} at 7 μM (0.7 ± 0.08; p = 0.03) (Fig. 9I-J).

DHA-glycine promotes the dose-dependent activation of Kv7.1/KCNE1 channels (Fig. 10A-B), left-shifting the voltage-dependence of activation (-10.5 ± 1.0 mV; p 0.002), and increasing the G_{max} at 7 μM (1.9 ± 0.2; p = 0.03) (Fig. 10C-D). However, DHA-glycine does not result in a dose-dependent decrease in Ca^{2+} currents (Fig. 10E). DHA-glycine does not left-shift the voltage dependence of inactivation (7.6 ± 3.1 mV; p = 0.13) and does not significantly decrease the G_{max} of Cav1.2 at 7 μM (1.0 ± 0.1; p = 0.98) (Fig. 10G). In addition, DHA-glycine produces some inhibition of Nav1.5, but only when applied at 20 μM (Fig. 10H). While DHA-glycine produces a small, but significant left-shift in voltage dependent inactivation at 7 μM (-4.8 ± 1.9 mV; p = 0.01), it does not significantly reduce the G_{max} at 7 μM (0.7 ± 0.08; p = 0.84) (Fig. 10H-J).

These results suggest that PUFA analogues with glycine head groups tend to be more selective for the cardiac Kv7.1/KCNE1 channel and tend to have lower apparent affinity for Cav1.2 and Nav1.5 channels. Pin-glycine and DHA-glycine both have more selective effects on the Kv7.1/KCNE1 channel and lower apparent affinity for Cav1.2 and Nav1.5 channels compared to PUFA analogues with taurine head groups. Lin-glycine, however, is less selective for Kv7.1/KCNE1 channels compared to Pin-glycine and DHA-glycine. Lin-glycine modulates Kv7.1/KCNE1 and Cav1.2 at similar concentrations, while the modulatory effects of Lin-glycine on Nav1.5 take place at higher concentrations. This suggests that the combination of a glycine head group and linoleic acid tail boosts the apparent affinity for Cav1.2 and Nav1.5 channels.

PUFA analogues with glycine head groups activate I_{Ks} with higher apparent affinity compared to I_{Ca} and I_{Na}.

We have observed that PUFA analogues have several different effects on the same channel (e.g. they alter voltage dependence and conductance at the same time). To evaluate the totally effects of PUFA analogues on channel currents at 0 mV (I/I_0), we compared the dose response curves for I_{Ks} (Kv7.1/KCNE1), I_{CaL} (Cav1.2), and I_{NaV} (Nav1.5) (Table 1). At 0 mV, 7 μM N-AT does not increase I_{Ks} currents, but instead inhibits I_{CaL} currents and almost completely inhibits I_{NaV} currents (Fig. 11A; Table 1). By comparing the dose response curves and K_m (a measure of apparent binding affinity) for each channel current, we find that N-AT has similar apparent affinity for I_{Ks}, I_{CaL}, and I_{NaV}. At 7 μM, Lin-taurine increases I_{Ks} (though not significantly) while significantly inhibiting I_{CaL} and I_{NaV}, and exhibits higher apparent affinity for I_{CaL} and I_{NaV} than for I_{Ks} (Fig. 11B; Table 1). Similar to Lin-taurine, Pin-taurine and DHA-taurine increase I_{Ks} but it also inhibit I_{CaL} and I_{NaV} with higher apparent affinity for I_{CaL} and I_{NaV} than for I_{Ks} (Fig. 11C-D; Table 1). At 7 μM, Lin-glycine increases I_{Ks}, but also inhibits I_{CaL} and I_{NaV} with higher apparent affinity for I_{CaL} than for I_{Ks} and I_{NaV} (Fig. 11E; Table 1). At 7 μM, Pin-glycine increases I_{Ks}, but does not significantly inhibit I_{CaL} or I_{NaV}. When we compare the K_m from the dose response curves of each channel current, we find that Pin-glycine has higher apparent affinity for I_{Ks} compared to I_{NaV} (Fig. 11F; Table 1). Lastly, at 7 μM, DHA-glycine increases I_{Ks} with little effect on I_{CaL} and I_{NaV}, exhibiting higher apparent affinity for I_{Ks} and I_{CaL} than for I_{NaV} (Fig. 11G; Table 1). Overall, when we compare the effects of different PUFA analogues on I_{Ks}, I_{NaV}, and I_{CaL}, PUFA analogues with taurine

head groups tend to have higher apparent affinity for I_{NaV} and I_{CaL}, whereas PUFA analogues with glycine head groups tend to have higher apparent affinity for I_{Ks}.

Selective Kv7.1/KCNE1 channel activators have antiarrhythmic effects in the simulated cardiomyocyte

We next tried to understand what kind of compound is the most effective at shortening the action potential duration. To determine whether selective PUFA analogues or non-selective PUFA analogues can shorten the action potential duration, we simulated the effects of applying the PUFA analogues on human cardiomyocyte using the O'Hara-Rudy dynamic (ORd) model (40) while modifying parameters for the voltage dependence and conductance for individual channels to reflect our experimental PUFA-induced effects. We simulated the effects of PUFA analogues that are non-selective modulators for cardiac ion channels (i.e. N-AT, Lin-taurine, Pin-taurine, DHA-taurine, and Lin-glycine) at concentrations of 0.7 μM, 2 μM, and 7 μM (Fig. 12A-E). In most cases, we saw little change in the ventricular action potential until we reached 7 μM where we were unable to elicit an action potential (Fig. 12A-E). One exception was the effect of applying DHA-taurine, in which case we observed a small shortening of the action potential at 0.7 μM, but then an abnormal action potential upstroke and prolongation of the action potential at 2 μM (Fig 12D). This is likely due to the potent block of Nav1.5 channels, causing the action potential to be largely calcium dependent. But again, at 7 μM DHA-taurine, we were unable to elicit an action potential (Fig. 12D). However, the PUFA analogues that were more selective for Kv7.1/KCNE1, such as Pin-glycine and DHA-glycine (at 7 μM) induce a slight shortening of the wild type ventricular

346 action potential (Fig. 12F-G). For Pin-glycine and DHA-glycine, we induced Long QT
347 Type 2 by simulating 25% block of the hERG channel, which generates the rapid
348 component of the delated rectifier potassium current (I_{Kr}). 25% hERG block prolongs the
349 ventricular action potential by 50 ms. Application of Pin-glycine or DHA-glycine at 7 μM
350 in the simulation partially restores the duration of the ventricular action potential. In
351 addition to simulating the effects of PUFA analogues on the ventricular action potential
352 duration, we also simulated the ability of 7 μM DHA-glycine (the most selective
353 Kv7.1/KCNE1 activator) to prevent arrhythmia by simulating early afterdepolarizations
354 using 0.1 μM dofetilide. Dofetilide is a blocker of the hERG channel and increases the
355 susceptibility for early afterdepolarizations (40) (Fig. 12H). When we simulate 0.1 μM
356 dofetilide + 7 μM DHA-glycine, we are able to suppress early afterdepolarizations,
357 suggesting that the application of 7 μM DHA-glycine would be anti-arrhythmic (Fig.
358 12H).
359
360 **Discussion**
361 We show here that PUFAs have different mechanisms of action on Kv7.1/KCNE1,
362 Cav1.2, and Nav1.5 channels. We have previously shown that PUFAs promote the
363 activation of Kv7.1/KCNE1 channels through the lipoelectric mechanism where the
364 negatively charged PUFA head group electrostatically attracts both the S4 voltage
365 sensor (facilitating its upward movement and channel opening) and K326 in S6
366 (increasing the maximal conductance) (36, 39, 42). In both Cav1.2 and Nav1.5
367 channels, PUFAs inhibit channel currents. We have found that PUFAs cause a dose-
368 dependent reduction in the currents through in Cav1.2 channels, surprisingly with no

effect on the voltage dependence of either activation or inactivation. In Nav1.5 channels, PUFAs cause inhibition through a dose-dependent decrease in currents, with both a left-shifting effect on the voltage dependence of inactivation and a decrease in conductance. We also demonstrate that PUFA analogues vary in their selectivity for voltage-gated ion channels. The selectivity depends on the specific concentration of PUFA applied, because several compounds have non-overlapping dose response curves for their effects on the three different channels (Fig. 11). We also found that PUFAs with taurine head groups tend to have broad modulatory effects on Kv7.1/KCNE1, Nav1.5 and Cav1.2 channels, with higher apparent affinity for Cav1.2 and Nav1.5 channels. Conversely, PUFAs with glycine head groups tend to be more selective for Kv7.1/KCNE1 channels and display lower apparent affinity for Cav1.2 and Nav1.5 channels. By understanding the effects of PUFA analogues on individual channels, it opens up the possibility to target specific forms of LQTS in which specific channels are mutated.

In this work, we have demonstrated that PUFA analogues modulate several different voltage-gated ion channels, including those underlying the ventricular action potential: Kv7.1/KCNE1, Nav1.5, and Cav1.2. The effects of PUFAs on Kv7.1/KCNE1, Cav1.2, and Nav1.5 individually are anticipated to have anti-arrhythmic effects and would potentially be beneficial for patients with Long QT Syndrome. In the case of I_{Ks} (Kv7.1/KCNE1) currents, PUFAs would be anti-arrhythmic by rescuing loss-of-function mutants of Kv7.1/KCNE1 (I_{Ks}) channels in Long QT Type 1 (KCNQ1 mutations) or 5 (KCNE1 mutations). In the case of Na_v and Ca_v currents, PUFAs would be anti-

arrhythmic by inhibiting gain-of-function mutants of Nav1.5 and Cav1.2 channels in Long QT Type 3 or 7, respectively. We used the O'Hara-Rudy Dynamic model to simulate the ventricular action potential in the presence of different PUFAs. In our simulations, PUFAs that are non-selective (i.e. that activate Kv7.1/KCNE1 while inhibiting Cav1.2 and Nav1.5) prevent the generation of an action potential. However, when we simulate the effects of Pin-glycine and DHA-glycine, which are both more selective for Kv7.1/KCNE1, we see a shortening in the action potential duration and the suppression of early afterdepolarizations. This suggests that selectively boosting I_{Ks} (Kv7.1/KCNE1) current would be important for shortening and terminating the ventricular action potential. However, evaluating PUFA-induced effects on Kv7.1/KCNE1, Cav1.2, and Nav1.5 channels bearing LQTS-causing mutations would be the next step in understanding the therapeutic potential for PUFA analogues as treatments for different forms of LQTS.

In our experiments using PUFA analogues on Nav1.5, we observed both a shift in the voltage dependence of inactivation and a dose-dependent decrease in Na^+ currents. Extensive work has been done to characterize how each of the different voltage-sensing domains in Nav channels contribute to voltage-dependent activation and inactivation, many implicating DIV S4 in fast inactivation (6, 43). Recent work by Hsu and colleagues (2017) has also shown using voltage clamp fluorometry, the importance of both DIII and DIV in Nav channel inactivation (44). Our data suggest that PUFAs may interact with S4 segments involved in voltage-dependent inactivation, allowing PUFA analogues to left-shift the voltage dependence of inactivation. However, this does not completely explain

the additional dose-dependent decrease in Na^+ currents we observe on top of the leftward shifted voltage dependence of inactivation. Recent work by Nguyen and colleagues (2018) has uncovered a mechanism of Na_v channel inhibition through a new pathway, allowing a hydrophobic molecules to permeate a fenestration between domains III and IV (DIII and DIV) in the human cardiac Nav1.5 channel (45). It is possible that the hydrophobic PUFA analogue also block Nav1.5 channels through this fenestration between DIII and DIV, causing the voltage-independent decrease in sodium currents.

The molecular mechanism of action of PUFA analogues on Cav1.2 is still unclear, though we have shown that it does not occur through a shift in the voltage dependence of inactivation. In each case of Cav1.2 inhibition by PUFA analogues, we observe a dose-dependent decrease in the Ca^{2+} currents that appears as a linear decrease in I/I_0 and G_{max}. There is evidence that some Ca_v channel antagonists, such as dihydropyridines (DHPs) inhibit Ca_v channels through an allosteric mechanism (46). Pepe and colleagues (1994) found that DHA alters the effectiveness of dihydropyridines, suggesting a shared binding site, or nearby binding sites, for DHPs and PUFAs (47). Tang and colleagues (2016) found that dihydropyridines bind in a hydrophobic pocket near the pore of the bacterial Ca_vAb channel and cause an allosteric conformational change that leads to disruption of the selectivity filter and thus inhibition of Ca^{2+} currents (46). In addition, they observed that in the absence of DHPs a phospholipid occupies the DHP binding site (46). This would suggest that it is possible that PUFA analogues inhibit Cav1.2 by binding to, or near, the DHP binding site and causing an allosteric conformational change that leads to a collapse of the pore and

438 thus explaining the inhibition of Cav1.2 currents without any changes in the voltage
439 dependence of inactivation.

440 Work from several groups has demonstrated a shared electrostatic mechanism of action
441 on voltage-gated K^+ channels (48) and voltage-gated Na^+ channels (49) by biaryl
442 sulfonamides. Liin and colleagues (2018) showed that biaryl sulfonamides promote the
443 activation of the Shaker K^+ channel through an electrostatic effect on the voltage sensing
444 domain. In addition, Ahuja and colleagues (2015) showed that aryl sulfonamides inhibit
445 Na_v channels through an electrostatic "voltage sensor trapping" mechanism that is
446 specific for the Nav1.7 isoform. The work by Ahuja et al. supports the ability to
447 pharmacologically target different ion channels with a high degree of selectivity (49). This
448 is in agreement with our findings using PUFA analogues that show that PUFA analogues
449 are variable in their channel selectivity, allowing us to target particular ion channels
450 involved in the ventricular action potential.

451 Our experiments were conducted using the *Xenopus laevis* oocyte expression system,
452 where voltage-clamp recordings were performed at room temperature. It is possible that
453 there may be temperature differences in the ways PUFA analogues modify different ion
454 channels that we are unable to capture by conducting experiments at 20ºC. There is
455 also the possibility that the membrane composition may differ between *Xenopus*
456 oocytes and mammalian cells or cardiomyocytes. However, using *Xenopus* oocytes, we
457 are able to measure distinct differences between mechanisms of PUFA modulation in
458 Kv7.1/KCNE1, Cav1.2, and Nav1.5 in isolation. To further confirm our findings,
459 experiments should be conducted in mammalian cells or cardiomyocytes to determine

460 the effects of different PUFA analogues on individual ion channels and the duration of
461 the ventricular action potential at physiological temperatures.

462 The work presented here demonstrates that PUFA analogues exert diverse modulatory
463 effects on different types of voltage-gated ion channels through non-identical
464 mechanisms. Because PUFA analogues modulate Kv7.1/KCNE1 channels through
465 electrostatic effects, we hypothesized they would have similar effects on Cav1.2 and
466 Nav1.5 channels. However, our data suggests that PUFA analogues can exert various
467 modulatory effects on the activity of different ion channels, and that the mechanism
468 depends on the ion channel that is being modulated. In addition, we have shown that
469 PUFA analogues exhibit a range of selectivity for different ion channels, which depends
470 both on the PUFA head group and the combination of PUFA head and tail groups. Using
471 simulations of the ventricular action potential, we have shown that selective Kv7.1/KCNE1
472 channel activators are the most effective at shortening a prolonged ventricular action
473 potential and suppressing early afterdepolarizations induced by hERG block. This
474 suggests that boosting Kv7.1/KCNE1 currents by using selective Kv7.1/KCNE1 channel
475 activators can aid in restoring a normal action potential duration and possess
476 antiarrhythmic potential.

477

478

Methods

Molecular Biology

cRNA encoding Kv7.1 and KCNE1, Nav1.5 and β1, and Cav1.2, β3, and α2δ were transcribed using the mMessage mMachine T7 kit (Ambion). 50 ng of cRNA was injected into defolliculated *Xenopus laevis* oocytes (Ecocyte, Austin, TX): For Kv7.1/KCNE1 channel expression, we injected a 3:1, weight:weight (Kv7.1:KCNE1) cRNA ratio. For Nav1.5 channel expression, we injected a 2:1, weight:weight (Nav1.5:β1) cRNA ratio. For Cav1.2 channel expression, we injected a 2:1:1, weight:weight (Cav1.2:β3:α2δ) cRNA ratio. Injected cells were incubated for 72-96 hours in standard ND96 solution (96 mM NaCl, 2 mM KCl, 1 mM $MgCl_2$, 1.8 mM $CaCl_2$, 5 mM HEPES; pH = 7.5) containing 1 mM pyruvate at 16ºC prior to electrophysiological recordings.

Two-electrode voltage clamp (TEVC)

Xenopus laevis oocytes were recorded in the two-electrode voltage clamp (TEVC) configuration. Recording pipettes were filled with 3 M KCl. The recording chamber was filled with ND96 (96 mM NaCl, 2 mM KCl, 1 mM $MgCl_2$, 1.8 mM $CaCl_2$, 5 mM HEPES; pH 7.5). For Cav1.2 channel recordings, *Xenopus* oocytes were injected with 50 nl of 100 mM EGTA and incubated at 10ºC for 30 minutes prior to electrophysiological recordings in order to sequester cytosolic calcium. In addition, Cav1.2 channel recordings were done in Ca^{2+}-free solutions, using Ba^{2+} as the charge carrier, to prevent calcium-dependent inactivation of Cav1.2 channels. PUFAs were obtained from Cayman Chemical (Ann Arbor, MI.) or synthesized in house (Linköping, Sweden) through methods previously described (Bohannon et al., submitted) and kept at -20˚C

as 100 mM stock solutions in ethanol. Serial dilutions of the different PUFAs were prepared from stocks to make 0.2 μM, 0.7 μM, 2 μM, 7 μM, and 20 μM concentrations in ND96 solutions (pH = 7.5). PUFAs were perfused into the recording chamber using the Rainin Dynamax Peristaltic Pump (Model RP-1) (Rainin Instrument Co., Oakland, CA. USA).

Electrophysiological recordings were obtained using Clampex 10.3 software (Axon, pClamp, Molecular Devices). To measure Kv7.1/KCNE1 currents we apply PUFAs as the membrane potential is stepped every 30 sec from -80 mV to 0 mV for 5 seconds before stepping to -40 mV and back to -80 mV to ensure that the PUFA effects on the current at 0 mV reached steady state. A voltage-step protocol was used to measure the current vs. voltage (I-V) relationship before PUFA application and after the PUFA effects had reached steady state for each concentration of PUFA. Cells were held at -80 mV followed by a hyperpolarizing prepulse to -140 mV. The voltage was then stepped from -100 to 60 mV (in 20 mV steps) followed by a subsequent voltage step to -20 mV to measure tail currents before returning to the -80 mV holding potential. For Cav1.2 channel recordings, PUFAs are applied as the membrane potential is stepped from -80 mV to -30 mV and then 10 mV before returning to the holding potential of -80 mV. This allows the PUFA effects to reach steady state before recording voltage-dependent activation and inactivation. To measure voltage-dependent activation of Cav1.2, cells are held again at -80 mV and then stepped from -70 mV to 40 mV (in 10 mV steps). Voltage-dependent inactivation was measured by holding cells at -80 mV, applying a 500-ms conditioning prepulse at voltages between -80 mV and 20 mV (in 10 mV steps)

before stepping to a test pulse of 10 mV to measure the remaining current and returning to -80 mV holding potential. For Nav1.5 channel recordings, PUFAs are applied as the membrane potential is stepped from -80 mV to -90 mV for 480 ms before stepping to 30 mV for 50 ms and returned to a holding potential of -80 mV. This allows the PUFA effects to reach steady state before recording voltage-dependent activation and inactivation. To measure voltage-dependent activation of Nav1.5, cells are held at -80 mV and then stepped from -90 mV to 40 mV (in 10 mV steps) and then returning to -80 mV holding potential. Voltage-dependent inactivation was measured by holding cells at -80 mV, applying a 500-ms conditioning prepulse at voltages between -140 mV and -30 mV (in 10 mV steps) and measuring the remaining current at a test pulse of -30 mV before returning to -80 mV holding potential.

539 *Data analysis*

540 Tail currents from Kv7.1/KCNE1 measures were analyzed using Clampfit 10.3 software
541 in order to obtain conductance vs. voltage (G-V) curves. The $V_{0.5}$, the voltage at which
542 half the maximal current occurs, was obtained by fitting the G-V curves from each
543 concentration of PUFA with a Boltzmann equation:

544 $$G(V) = \frac{Gmax}{1 + e^{\frac{(V_{\frac{1}{2}} - V)}{s}}}$$

545 where G_{max} is the maximal conductance at positive voltages and s is the slope factor in
546 mV. The current values for each concentration at 0 mV (I/I_0) were used to plot the dose
547 response curves for each PUFA. These dose response curves were fit using the Hill
548 equation in order to obtain the K_m value for each PUFA:

549

550 $$\frac{I}{I_0} = 1 + \frac{A}{1 + \frac{Km^n}{x^n}}$$

551

552 where A is the fold increase in the current caused by the PUFA at saturating
553 concentrations, K_m is the apparent affinity of the PUFA, and n is the Hill coefficient. The
554 maximum conductance (G_{max}) was calculated by taking the difference between the
555 maximum and minimum current values (using the G-V curve for each concentration)
556 and then normalizing to control solution (0 μM). In Cav1.2 and Nav1.5 channels, peak
557 currents (normalized to the peak values in control ND96) were used to determine PUFA
558 induced changes in I/I_0, $\Delta V_{0.5}$ of inactivation, and G_{max}. Graphs plotting I/I_0, $\Delta V_{0.5}$, G_{max},
559 and K_m were generated using the Origin 9 software (Northampton, MA.). To determine if
560 there were significant differences between apparent binding affinity of individual PUFA

561 analogues for Kv7.1/KCNE1, Cav1.2, or Nav1.5 we conducted One-way ANOVA
562 followed by Tukey's HSD for multiple comparisons when comparing all three channels
563 or Student's t-test when comparing the apparent affinity for two channels. To determine
564 if the PUFA-induced effects on I/I_0, $\Delta V_{0.5}$, or G_{max} were statistically significant we
565 conducted Student's t-test on the PUFA-induced effects at 7 μM. Significance α-level
566 was set at $p < 0.05$ – asterisks denote significance: $p < 0.05$*, $p < 0.01$**, $p < 0.001$***, p
567 < 0.0001****.
568
569 *Simulations*
570 The effects of individual PUFA analogues were simulated on each ion channel using
571 Berkeley Madonna modeling software and equations from the MATLAB code in the
572 O'Hara and Rudy Dynamic (ORd) model (40). We individually simulated the
573 Kv7.1/KCNE1, Cav1.2, and Nav1.5 channels in Madonna and altered the parameters
574 suggested to be modulated by PUFA binding to recapitulate our voltage clamp data
575 from *Xenopus* oocytes. For example, to model the effects observed on the cardiac I_{Ks}
576 channel, we modified the voltage dependence of channel activation by shifting the $V_{0.5}$
577 as well as multiplying the I_{Ks} conductance by the factor increase we observed in our
578 experiments at a given PUFA concentration.
579
580 MATLAB simulations of the ventricular action potential in the epicardium of the heart
581 were performed using the ORd model (40). To simulate the effects of PUFAs, we
582 introduced the same modified parameters in the MATLAB code as we used to model
583 the PUFA effects on the ionic currents in Berkeley Madonna. We made simultaneous
584 changes to Kv7.1/KCNE1, Cav1.2, and Nav1.5 for a given PUFA and specific PUFA

585 concentration to model the effects of different PUFA analogues on the ventricular action
586 potential under wild type and LQTS conditions. To simulate susceptibility to early
587 afterdepolarizations, hERG block by 0.1 μM dofetilide was simulated which previously
588 has been shown to cause spontaneous early afterdepolarizations (40). To simulate the
589 ability of PUFA analogues to suppress early afterdepolarizations, we altered the activity
590 of Kv7.1/KCNE1, Cav1.2, and Nav1.5 channels according to the PUFA-induced effects
591 observed during experiments.
592
593

Acknowledgements

We thank Levi Lindroos, Victor Kornfeld, Siri Lundholm, and Sankhero Gewarges for their contributions during their time as visiting scholars.

Conflict of Interest

SIL, HPL: A patent application (62/032,739) has been submitted by the University of Miami with SIL and HPL as inventors. The other authors declare no other competing interests.

Author Contributions

BMB, Acquisition of data, Analysis and interpretation of data, Drafting or revising the article; HPL, Conception and design, Analysis and interpretation of data, Drafting or revising the article; SIL, Conception and design, Acquisition of data, Analysis and interpretation of data, Drafting or revising the article; MEP, Acquisition of data; XW, Acquisition of data.

Funding

This work was supported by NIH R01-HL131461 (to H. Peter Larsson) and by the Swedish Society for Medical Research and the Swedish Research Council (2017-02040) (to Sara I. Liin).

References

1. Mohrman D, Heller L. Cardiovascular Physiology. 7 ed: McGraw Hill Co.; 2010.
2. Nerbonne J, Kass R. Molecular Physiology of Cardiac Repolarization. Physiological Reviews. 2005;85:1205-53. doi: doi:10.1152/physrev.00002.2005.
3. Alders M, Christiaans I. Long QT Syndrome. Gene Reviews. 2003.
4. Bohnen M, Peng G, Robey S, Terrenoire C, Iyer V, Sampson K, Kass R. Molecular Pathophysiology of Congenital Long QT Syndrome. Physiology Reviews. 2017;97:46.
5. Chanda B, Bezanilla F. Tracking Voltage-dependent Conformational Changes in Skeletal Muscle Sodium Channel during Activation. Journal of General Physiology. 2002;120:629-45.
6. Capes D, Goldschen-Ohm M, Arcisio-Miranda M, Bezanilla F, Chanda B. Domain IV voltage-sensor movement is both sufficient and rate limiting for fast inactivation in sodium channels. Journal of General Physiology. 2013;142:101-12.
7. Barro-Soria R, Liin S, Larsson H. Using fluorescence to understand β subunit-Nav channel interactions. The Journal of General Physiology. 2017;149:757-62.
8. Xiao Y, Wright S, Wang G, Morgan J, Leaf A. Coexpression with β_1-subunit modifies the kinetics and fatty acid block of hH1$_\alpha$ Na^+ channels. American Journal of Physiology. 2000;279:12.
9. Zhu W, Voelker T, Varga Z, Schubert A, Nerbonne J, Silva J. Mechanisms of noncovalent β subunit regulation of Nav channel gating. The Journal of General Physiology. 2017;149:813-31.
10. Fernandez-Falgueras A, Sarquella-Brugada G, Brugada J, Brugada R, Campuzano O. Cardiac Channelopathies and Sudden Death: Recent Clinical and Genetic Advances. Biology. 2017;6:21.
11. Calloe K, Refaat M, Grubb S, Wojciak J, Campagna J, Thomsen N, Nussbaum R, Scheinman M, Schmitt N. Characterization and Mechanisms of Action of Novel Nav1.5 Channel Mutations Associated with Brugada Syndrome. Circulation Arrhythmia Electrophysiology. 2013:177-84. doi: DOI: 10.1161/CIRCEP.112.974220.
12. Rivolta I, Clancy C, Tateyama M, Liu H, Priori S, Kass R. A novel SCN5A mutation associated with long QT-3: altered inactivation kinetics and channel dysfunction. Physiological Genomics. 2002;10:191-7.
13. Rougier J, Abriel H. Cardiac voltage-gated calcium channel macromolecular complexes. Biochimica et Biophysica Acta. 2016;1863:1806-12.
14. Chen Y, Li M, Zhang Y, He L, Yamada Y, Fitzmaurice A, Shen Y, Zhang H, Tong L, Yang J. Structural basis of the α1-β subunit interaction of voltage-gated Ca^{2+} channels. Nature. 2004;429:675-80.
15. Stotz S, Jarvis S, Zamponi G. Functional roles of cytoplasmic loops and pore lining transmembrane helices in the voltage-dependent inactivation of HVA calcium channels. Journal of Physiology. 2003;554.2:263-73.
16. Zhang J, Ellinor T, Aldrich R, Tsien R. Molecular determinants of voltage-dependent inactivation in calcium channels. Letters to Nature. 1994;372:4.
17. Dick I, Joshi-Mukherjee R, Yang W, Yue D. Arrhythmogenesis in Timothy Syndrome is associated with defects in Ca^{2+}-dependent inactivation. Nature Communications. 2016;7. doi: 10.1038/ncomms1037.
18. Hoffman E. Voltage-Gated Ion Channelopathies: Inherited Disorders Caused by Abnormal Sodium, Chloride, and Calcium Regulation in Skeletal Muscle. Annual Reviews Medicine. 1995;46:10.
19. Noble D, Tsien R. Reconstruction of the Repolarization Process in Cardiac Purkinje Fibres Based on Voltage Clamp Measurements of Membrane Current. Journal of Physiology. 1969;200:22.
20. Deal KK, England SK, Tamkun MM. Molecular Physiology and Cardiac Potassium Channels. Physiological Reviews. 1996;76(1):49-67.
21. Lei M, Brown H. Two Components of the Delayed Rectifier Potassium Current, I_K, in Rabbit Sino-Atrial Node Cells. Experimental Physiology. 1996;81:16.

662 22. Barro-Soria R, Rebolledo S, Liin SI, Perez ME, Sampson KJ, Kass RS, Larsson HP. KCNE1 divides the
663 voltage sensor movement in KCNQ1/KCNE1 channels into two steps. Nature Communications.
664 2014;5:3750. doi: 10.1038/ncomms4750

665 https://www.nature.com/articles/ncomms4750#supplementary-information.
666 23. Osteen J, Gonzalez C, Sampson K, Iyer V, Rebolledo S, Larsson H, Kass R. KCNE1 alters the
667 voltage sensor movements necessary to open the KCNQ1 channel gate. Proceedings of the National
668 Academy of Sciences. 2010;107:6.
669 24. Huang H, Kuenze G, Smith J, Vanoye, CG., George Jr., AL., Meiler, J., Sanders, CR., Taylor K,
670 Duran A, Hadziselimovic A, Meiler J, Vanoye C, George A, Sanders C. Mechanisms of KCNQ1 channel
671 dysfunction in long QT syndrome involving voltage sensor domain mutations. Science Advances.
672 2018;4:13.
673 25. Ma D, Wei H, Lu J, Huang D, Liu Z, Loh L, Islam O, Liew R, Shim W, Cook S. Characterization of a
674 novel KCNQ1 mutation for type 1 long QT syndrome and assessment of therapeutic potential of a novel
675 IKs activator using patient-specific induced pluripotent stem cell-derived cardiomyocytes. Stem Cell
676 Research and Therapy. 2015;6:1-13.
677 26. Schwartz P, Crotti L, Insolia R. Long QT Syndrome: From Genetics to Management. Circulation:
678 Arrhythmia and Electrophysiology. 2012;5(4):9.
679 27. Sanguinetti M. Dysfunction of Delayed Rectifier Potassium Channels in an Inherited Cardiac
680 Arrhythmia. Annals of the New York Academy of Sciences. 1999;868:406-12. doi: 10.1111/j.1749-
681 6632.1999.tb11302.x.
682 28. Harmer S, Wilson A, Aldridge R, Tinker A. Mechanisms of disease pathogenesis in long QT
683 syndrome type 5. American Journal of Cell Physiology. 2009;298:C263-C73.
684 29. Endo J, Arita M. Cardioprotective mechanism of omega-3 polyunsaturated fatty acids. Journal of
685 Cardiology. 2016;67:5.
686 30. Kang J, Leaf A. Prevention of fatal cardiac arrythmias by polyunsaturated fatty acids. The
687 American Journal of Clinical Nutrition. 2000;71:6.
688 31. Benatti P, Peluso G, Nicolai R, Calvani M. Polyunsaturated Fatty Acids: Biochemical, Nutritional,
689 and Epigenetic Properties. Journal of the American College of Nutrition. 2004;23:281-302.
690 32. Kang J, Leaf A. Evidence that free polyunsaturated fatty acids modify Na^+ channels by directly
691 binding to the channel proteins. Proceedings of the National Academy of Sciences. 1996;93:3542-6.
692 33. Xiao Y, Gomez, AM., Morgan, JP., Lederer, WJ., Leaf, A. Suppression of voltage-gated L-type Ca^{2+}
693 currents by polyunsaturated fatty acids in adult and neonatal rat ventricular myocytes. Proceedings of
694 the National Academy of Sciences. 1997;94:6.
695 34. Xiao YF, Kang JX, Morgan JP, Leaf A. Blocking effects of polyunsaturated fatty acids on Na^+
696 channels of neonatal rat cardiomyocytes. Proceedings of the National Academy of Sciences.
697 1995;92:11000-4.
698 35. Xiao Y, Qingen K, Wang S, Auktor K, Yang Y, Wang G, Morgan J, Leaf A. Single point mutations
699 affect fatty acid block of human myocardial sodium channel a subunit Na^+ channels. Proceedings of the
700 National Academy of Sciences. 2001;98(6):6.
701 36. Borjesson S, Hammarstrom S, Elinder F. Lipoelectric Modification of Ion Channel Voltage Gating
702 by Polyunsaturated Fatty Acids. Biophysical Journal. 2008;95:11.
703 37. Liin S, Ejneby M, Barro-Soria R, MA. S, Larsson J, Harlin F, Parkkari T, Bentzen B, Schmitt N,
704 Larsson H, Elinder F. Polyunsaturated fatty acid analogs act antiarrhythmically on the cardiac I_{Ks} channel.
705 Proceedings of the National Academy of Sciences. 2015;112(18):6.
706 38. Liin S, Larsson J, Barro-Soria R, Bentzen B, Larsson H. Fatty acid analogue N-arachidonoyl taurine
707 restores function of I_{Ks} channels with diverse long QT mutations. eLIFE. 2016. doi:
708 dx.doi.org/10.7554/eLife.20272.

709 39. Liin S, Yazdi S, Ramentol R, Barro-Soria R, Larsson H. Mechanisms Underlying the Dual Effect of
710 Polyunsaturated Fatty Acid Analogs on Kv7.1. Cell Reports. 2018;24:2908-18. doi:
711 doi.org/10.1016/j.celrep.2018.08.031.
712 40. O'Hara T, Virag L, Varro A, Rudy Y. Simulation of the Undiseased Human Cardiac Ventricular
713 Action Potential: Model Formulation and Experimental Validation. PLOS Computational Biology.
714 2011;7(5):29. doi: doi:10.1371/journal.pcbi.1002061.
715 41. Larsson J, Larsson H, Liin S. KCNE1 tunes the sensitivity of Kv7.1 to polyunsaturated fatty acids
716 by moving turret residues close to the binding site. eLIFE. 2018. doi: doi.org/10.7554/eLife.37257.
717 42. Borjesson S, Elinder F. An electrostatic potassium channel opener targeting the final voltage
718 sensor transition. Journal of General Physiology. 2011;137:563-77. doi: DOI: 10.1085/jgp.201110599.
719 43. Ahern C, Payandeh J, Bosmans F, Chanda B. The hitchhiker's guide to the voltage-gated sodium
720 channel galaxy. Journal of General Physiology. 2015;147:1-24. doi: DOI: 10.1085/jgp.201511492.
721 44. Hsu E, Zhu W, Schubert A, Voelker T, Varga Z, Silva J. Regulation of Na^+ channel inactivation by
722 the DIII and DIV voltage-sensing domains. Journal of General Physiology. 2017;149:389-403. doi:
723 doi.org/10.1085/jgp.201611678.
724 45. Nguyen P, DeMarco K, Vorobyov I, Clancy C, Yarov-Yarovoy V. Structural basis for antiarrhythmic
725 drug interactions with the human cardiac sodium channel. Proceedings of the National Academy of
726 Sciences. 2019;116:2945-54. doi: doi.org/10.1073/pnas.1817446116.
727 46. Tang L, Gamal El-Din T, Swanson T, Pryde D, Scheuer T, Zheng N, Catterall W. Structural basis for
728 inhibition of a voltage-gated Ca^{2+} channel by Ca^{2+} antagonist drugs. Nature Letters. 2016;537:16.
729 47. Pepe S, Bogdanov K, Hallaq H, Spurgeon H, Leaf A, Lakatta E. ω3 polyunsaturated fatty acid
730 modulates dihydropyridine effects on L-type Ca^{2+} channels, cytosolic Ca^{2+}, and contraction in adult rat
731 cardiac myocytes. Proceedings of the National Academy of Sciences. 1994;91:8832-6.
732 48. Liin S, Lund P, Larsson J, Brask J, Wallner B, Elinder F. Biaryl sulfonamide motifs up- or down-
733 regulate ion channel activity by activating voltage sensors. Journal of General Physiology.
734 2018;150:1215-30. doi: DOI: 10.1085/jgp.201711942.
735 49. Ahuja S, Mukund S, Deng L, Khakh K, Chang E, Ho H, Shriver S, Young C, Lin S, Johnson Jr. J, Wu
736 P, Li J, Coons M, Tam C, Brillantes B, Sampang H, Mortara K, Bowman K, Clark K, Estevez A, Xie Z,
737 Verschoof H, Grimwood M, Dehnhardt C, Andrez J, Focken T, Sutherlin D, Safina B, Starovasnik M,
738 Ortwine D, Franke Y, Cohen C, Hackos D, Koth C, Payandeh J. Structural basis of Nav1.7 inhibition by an
739 isoform-selective small-molecule antagonist. Science. 2015;350(6267):1491-502.

740

741

Table 1: Summary of PUFA effects on current and apparent affinity

PUFA	I_{Ks} I/I_0 (at 7 µM) (mean ± SEM)	K_m I_{Ks} (µM) (mean ± SEM)	I_{Ca} I/I_0 (at 7 µM) (mean ± SEM)	K_m I_{Ca} (µM) (mean ± SEM)	I_{Na} I/I_0 (at 7 µM) (mean ± SEM)	K_m I_{Na} (µM) (mean ± SEM)
N-AT	1.12 ± 0.1 (p = 0.27)	9.8 ± 3.3	0.5 ± 0.1 (p = 0.04)	3.4 ± 2.5	0.2 ± 0.01 (p = 0.001)	3.1 ± 0.3
Lin-taurine	7.7 ± 2.9 (p = 0.14)	11.4 ± 0.4	0.3 ± 0.1 (p = 0.02)	0.1 ± 0.01	0.1 ± 0.02 (p = 0.0001)	2.4 ± 0.04
Pin-taurine	6.8 ± 1.0 (p = 0.01)	4.5 ± 0.2	0.7 ± 0.1 (p = 0.02)	NA	0.5 ± 0.1 (p = 0.01)	5.8 ± 1.7
DHA-taurine	5.1 ± 0.7 (p = 0.03)	5.9 ± 0.3	0.3 ± 0.05 (p = 0.02)	0.9 ± 0.6	0.07 ± 0.01 (p = 0.0001)	2.3 ± 0.1
Lin-glycine	5.1 ± 0.4 (p = 0.002)	5.4 ± 0.2	0.4 ± 0.2 (p = 0.07)	2.2 ± 0.5	0.5 ± 0.1 (p = 0.02)	5.6 ± 0.5
Pin-glycine	2.5 ± 0.2 (p = 0.02)	3.8 ± 0.4	0.8 ± 0.1 (p = 0.26)	NA	0.7 ± 0.1 (p = 0.09)	7.1 ± 1.2
DHA-glycine	3.7 ± 1.0 (p = 0.07)	9.4 ± 0.5	0.9 ± 0.1 (p = 0.19)	0.9 ± 0.03	1.1 ± 0.05 (p = 0.24)	16.7 ± 0.1

I/I_0 represents the relative current of the specified channel. The K_m indicates the concentration at which half the maximal effect on I/I_0 occurs and is used as a measure of the apparent affinity of the PUFA analogue. Data is represented at the mean ± SEM. Comparisons were made using One-way ANOVA and Student's t t-test. Significance level is set to p = 0.05.

742

743 **Figures and Figure Legends**

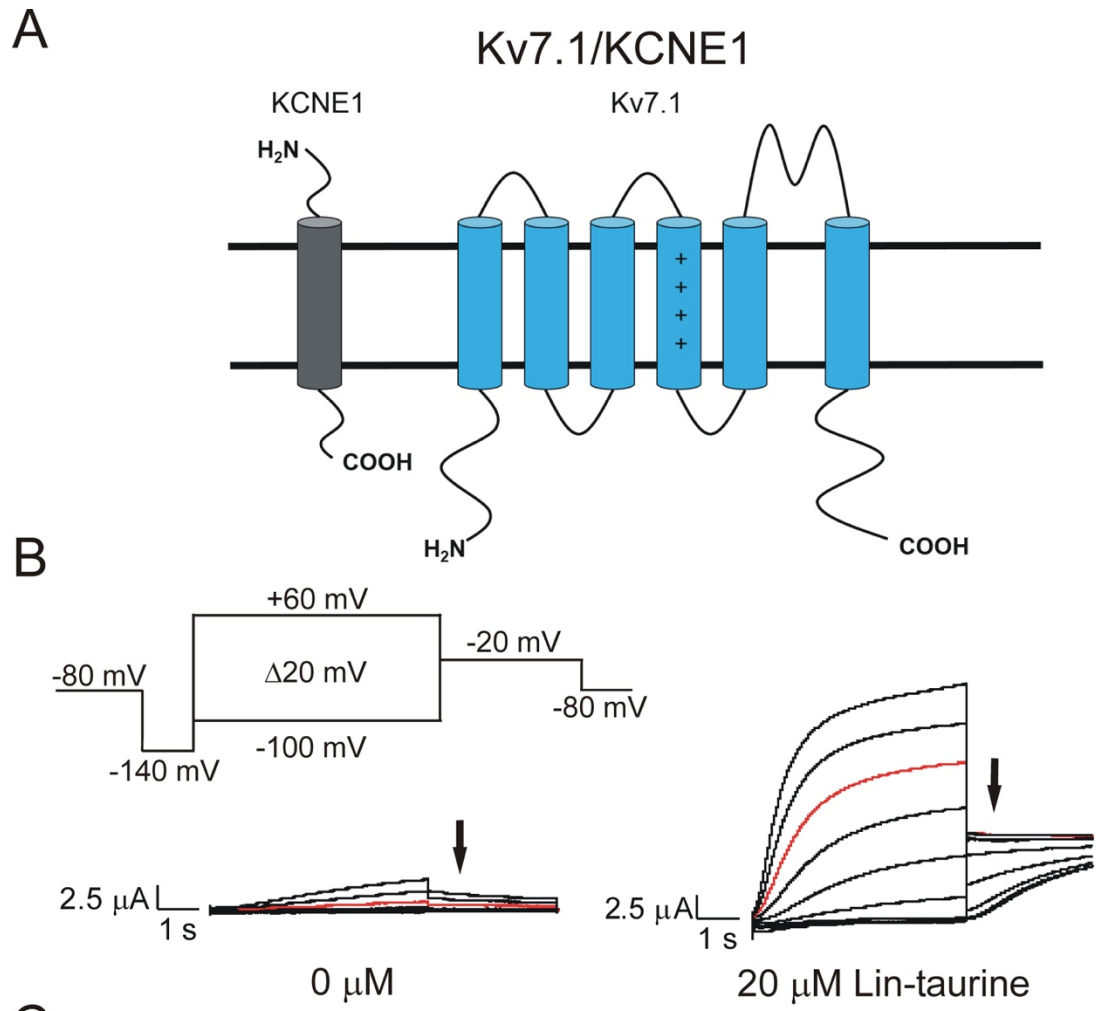

744

745

746 **Figure 1: PUFAs activate Kv7.1/KCNE1 channels through an electrostatic**
747 **mechanism on voltage sensor and pore. A)** Simplified membrane topology of a
748 single Kv7.1 α-subunit (blue) and a single KCNE1 β-subunit (grey). **B)** Voltage protocol
749 used to measure voltage dependence of activation and representative Kv7.1/KCNE1
750 current traces in control (0 μM) and 20 μM Lin-taurine. Arrows mark tail currents. **C)**
751 Current-voltage relationship demonstrating PUFA induced left-shift in the voltage-
752 dependence of activation ($V_{0.5}$) and increase in maximal conductance (G_{max}) (mean ±
753 SEM; n = 3).

754

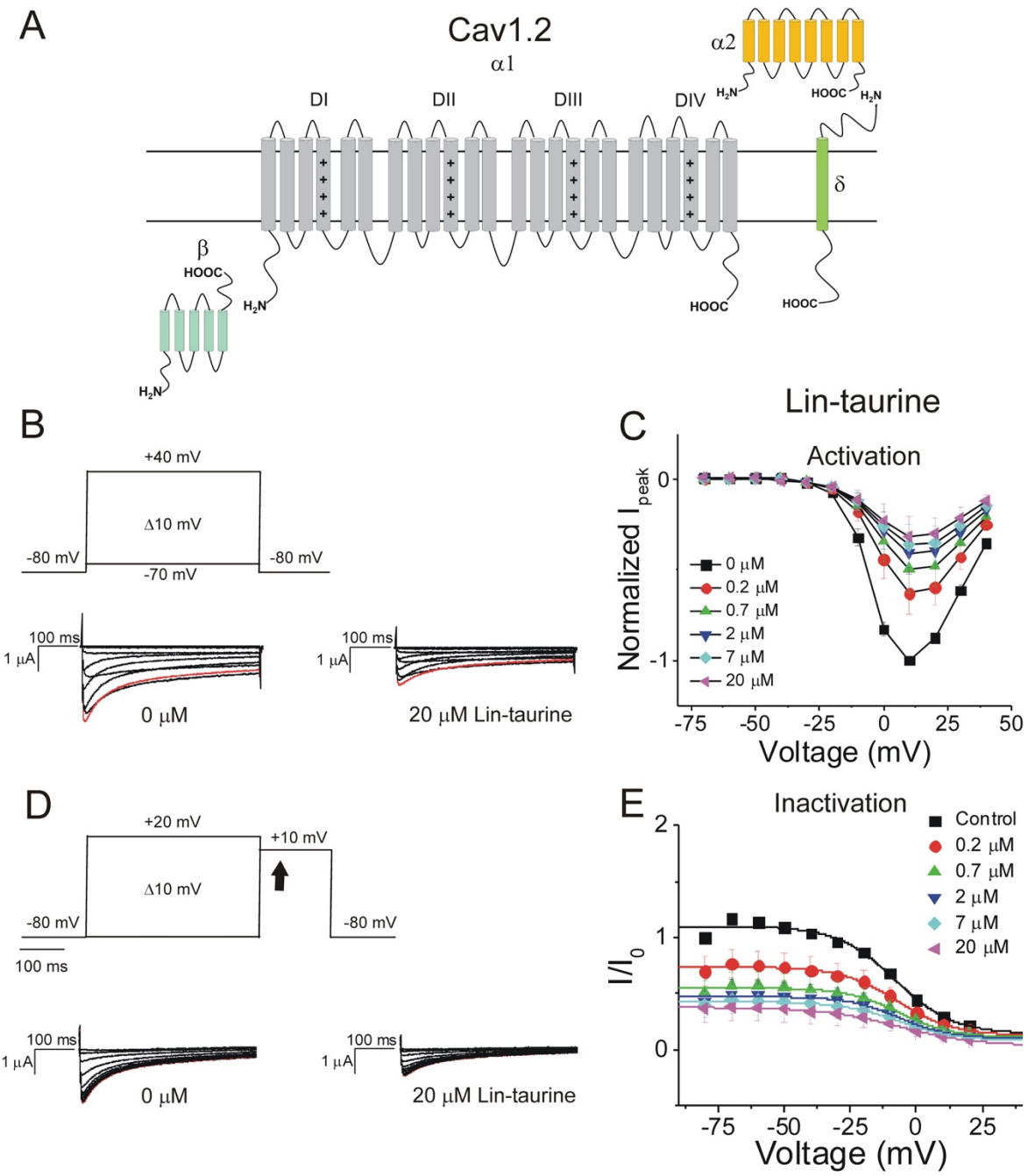

755

Figure 2: PUFAs inhibit Cav1.2 channels without altering channel voltage dependence. A) Simplified membrane topology of the Cav1.2 pore-forming α-subunit (light gray) and auxiliary β- (mint) and α2δ-subunits (yellow and green). **B)** Voltage protocol used to measure voltage dependence of activation and representative Cav1.2 current traces in control (0 μM) and 20 μM Lin-taurine. **C)** Current-voltage relationship demonstrating dose-dependent inhibition of Cav1.2 currents measured from activation protocol (mean ± SEM; n = 3). **D)** Voltage protocol used to measure voltage dependence of inactivation and representative Cav1.2 current traces in control (0 μM) and 20 μM Lin-taurine measured at arrow. **E)** Current-voltage relationship demonstrating dose-dependent inhibition of Cav1.2 currents measured from inactivation protocol (mean ± SEM; n = 3).

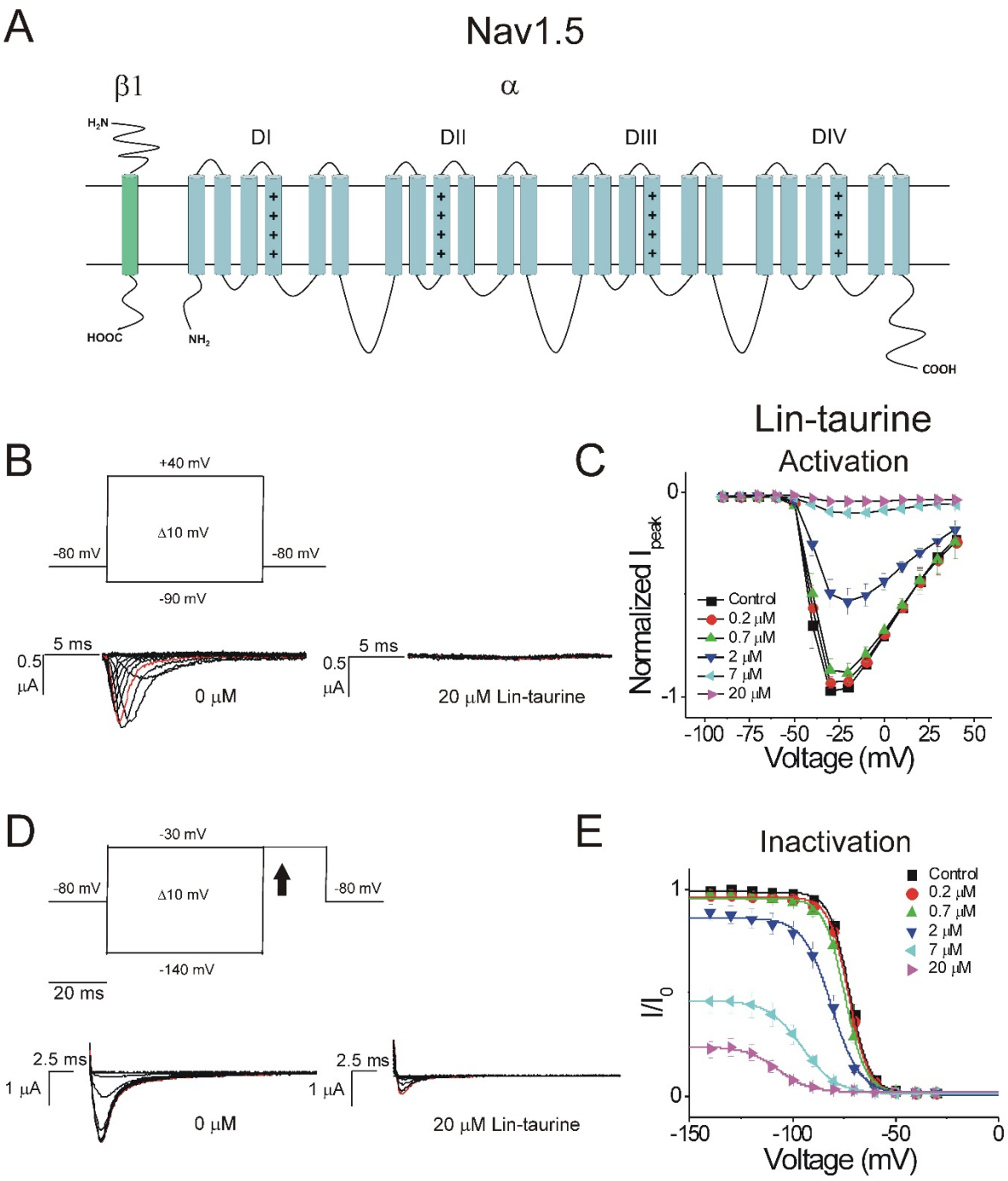

768

769 **Figure 3: PUFAs inhibit Nav1.5 by shifting the voltage dependence of inactivation.**
770 **A)** Simplified membrane topology of the Nav1.5 pore-forming α-subunit (light blue) and
771 auxiliary β-subunit (green). **B)** Voltage protocol used to measure voltage dependence of
772 activation and representative Nav1.5 current traces in control (0 μM) and 20 μM Lin-
773 taurine. **C)** Current-voltage relationship demonstrating dose-dependent inhibition of
774 Nav1.5 currents measured from activation protocol (mean ± SEM; n = 5). **D)** Voltage
775 protocol used to measure voltage dependence of inactivation and representative Nav1.5
776 current traces in control (0 μM) and 20 μM Lin-taurine measured at arrow. **E)** Current-
777 voltage relationship demonstrating dose-dependent inhibition of Nav1.5 currents and
778 leftward shift in the voltage dependence of inactivation measured from inactivation
779 protocol (mean ± SEM; n = 5).

780

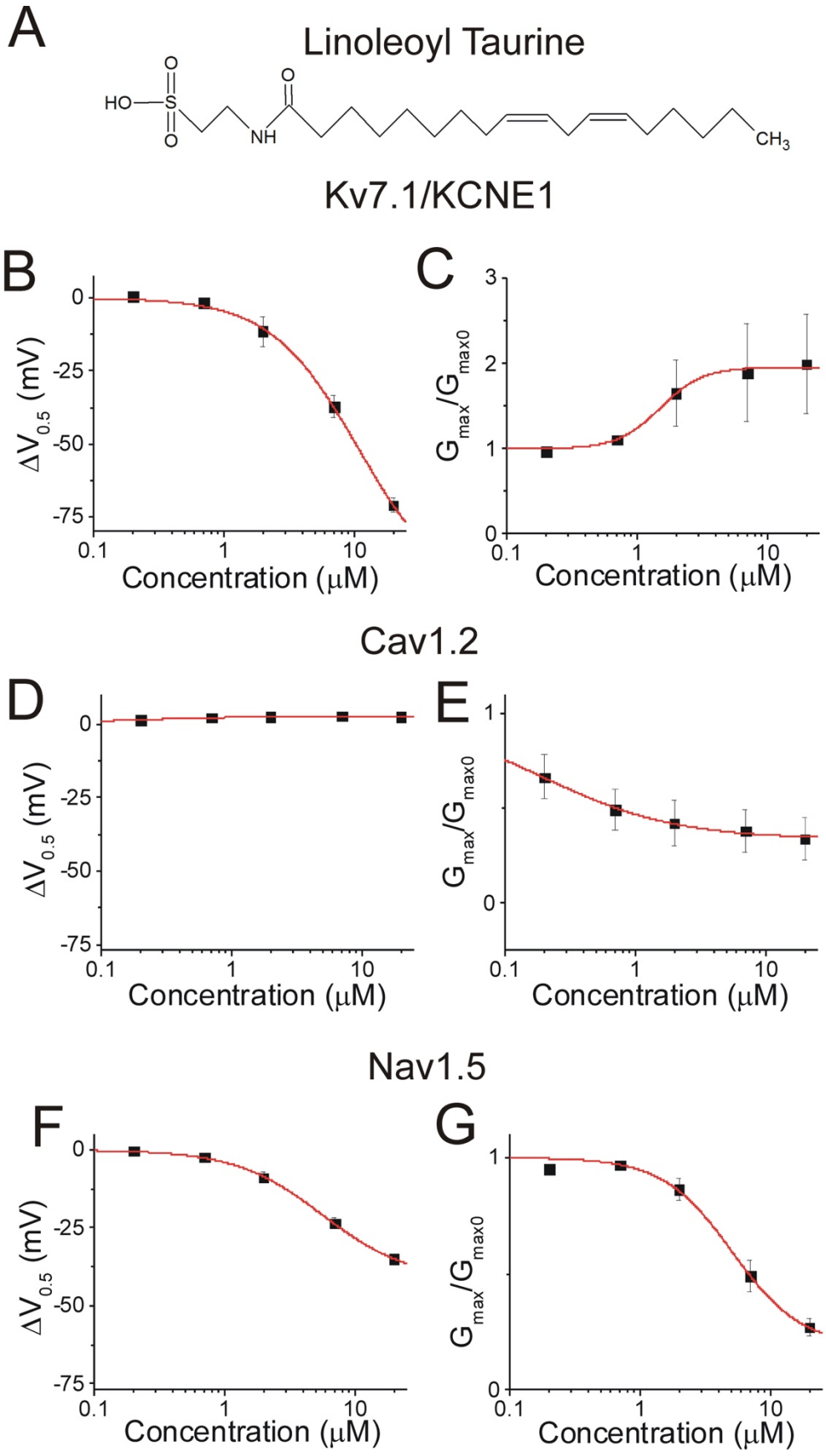

Figure 4: Linoleoyl taurine has broad selectivity for Kv7.1/KCNE1, Cav1.2, and Nav1.5. A) Structure of Linoleoyl taurine (Lin-taurine). **B, D, F)** Dose response of the shift in voltage dependent **B)** activation ($\Delta V_{0.5}$) of Kv7.1/KCNE1 channels (mean ± SEM; n = 3), **D)** inactivation ($\Delta V_{0.5}$) of Cav1.2 channels (mean ± SEM; n = 3), **F)** inactivation ($\Delta V_{0.5}$) of Nav1.5 channels (mean ± SEM; n = 5) in the presence of lin-taurine. **C, E, G)** Dose response of the change in maximal conductance (G_{max}) of **C)** Kv7.1/KCNE1 channels **E)** Cav1.2 channels, **G)** Nav1.5 channels in the presence of lin-taurine.

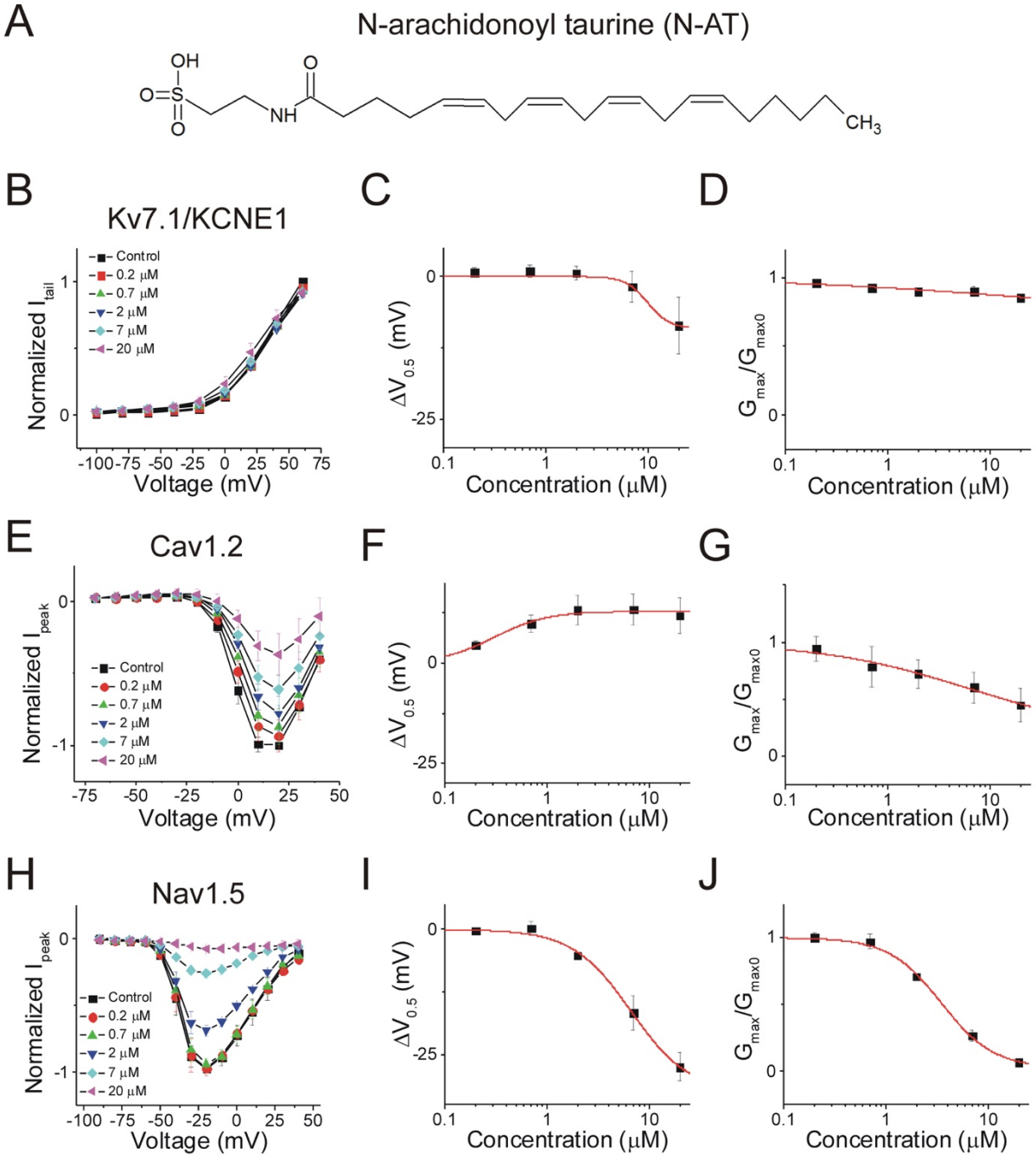

791

Figure 5: N-arachidonoyl taurine is more selective for Cav1.2 and Nav1.5 than for Kv7.1/KCNE1. A) Structure of N-arachidonoyl taurine (N-AT). **B)** Current-voltage relationship of N-AT on Kv7.1/KCNE1 channels (mean ± SEM; n = 5). **C)** Dose response of the shift in voltage dependent activation ($\Delta V_{0.5}$) of Kv7.1/KCNE1 channels in the presence of N-AT. **D)** Dose response of the change in maximal conductance (G_{max}) of Kv7.1/KCNE1 channels in the presence of N-AT. **E)** Current-voltage relationship of N-AT on Cav1.2 channels (mean ± SEM; n = 4). **F)** Dose response of the shift in voltage dependent inactivation ($\Delta V_{0.5}$) of Cav1.2 channels in the presence of N-AT. **G)** Dose response of the change in maximal conductance (G_{max}) of Cav1.2 channels in the presence of N-AT. **H)** Current-voltage relationship of N-AT on Nav1.5 channels (mean ± SEM; n = 3). **I)** Dose response of the shift in voltage dependent inactivation ($\Delta V_{0.5}$) of Nav1.5 channels in the presence of N-AT. **J)** Dose response of the change in maximal conductance (G_{max}) of Nav1.5 channels in the presence of N-AT.

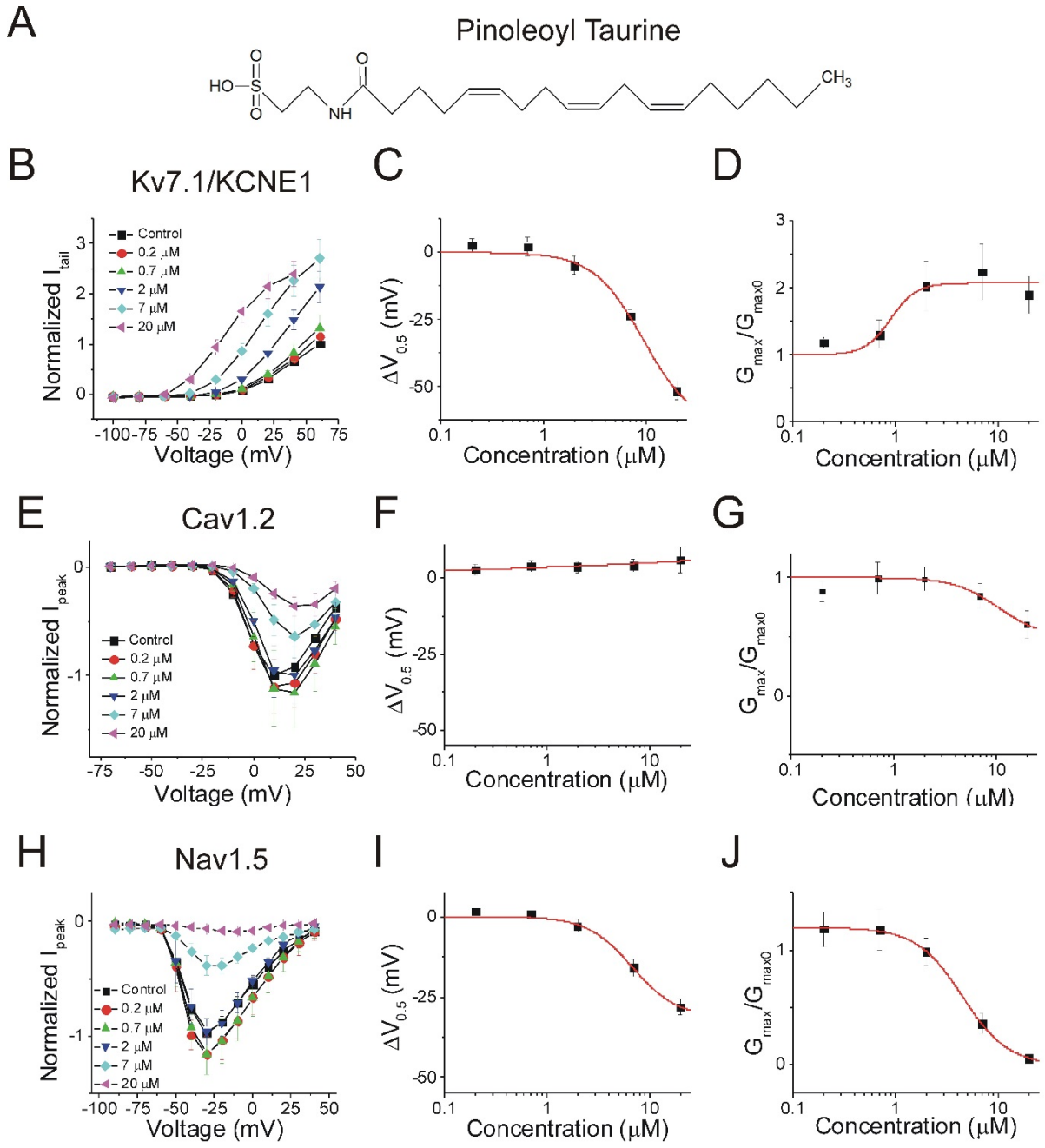

805

Figure 6: Pinoleoyl taurine has broad selectivity for Kv7.1/KCNE1, Cav1.2, and Nav1.5. A) Structure of Pinoleoyl taurine (Pin-taurine). **B)** Current-voltage relationship of pin-taurine on Kv7.1/KCNE1 channels (mean ± SEM; n = 4). **C)** Dose response of the shift in voltage dependent activation ($\Delta V_{0.5}$) of Kv7.1/KCNE1 channels in the presence of pin-taurine. **D)** Dose response of the change in maximal conductance (G_{max}) of Kv7.1/KCNE1 channels in the presence of pin-taurine. **E)** Current-voltage relationship of pin-taurine on Cav1.2 channels (mean ± SEM; n = 5). **F)** Dose response of the shift in voltage dependent inactivation ($\Delta V_{0.5}$) of Cav1.2 channels in the presence of pin-taurine. **G)** Dose response of the change in maximal conductance (G_{max}) of Cav1.2 channels in the presence of pin-taurine. **H)** Current-voltage relationship of pin-taurine on Nav1.5 channels (mean ± SEM; n = 4). **I)** Dose response of the shift in voltage dependent inactivation ($\Delta V_{0.5}$) of Nav1.5 channels in the presence of pin-taurine. **J)** Dose response of the change in maximal conductance (G_{max}) of Nav1.5 channels in the presence of pin-taurine.

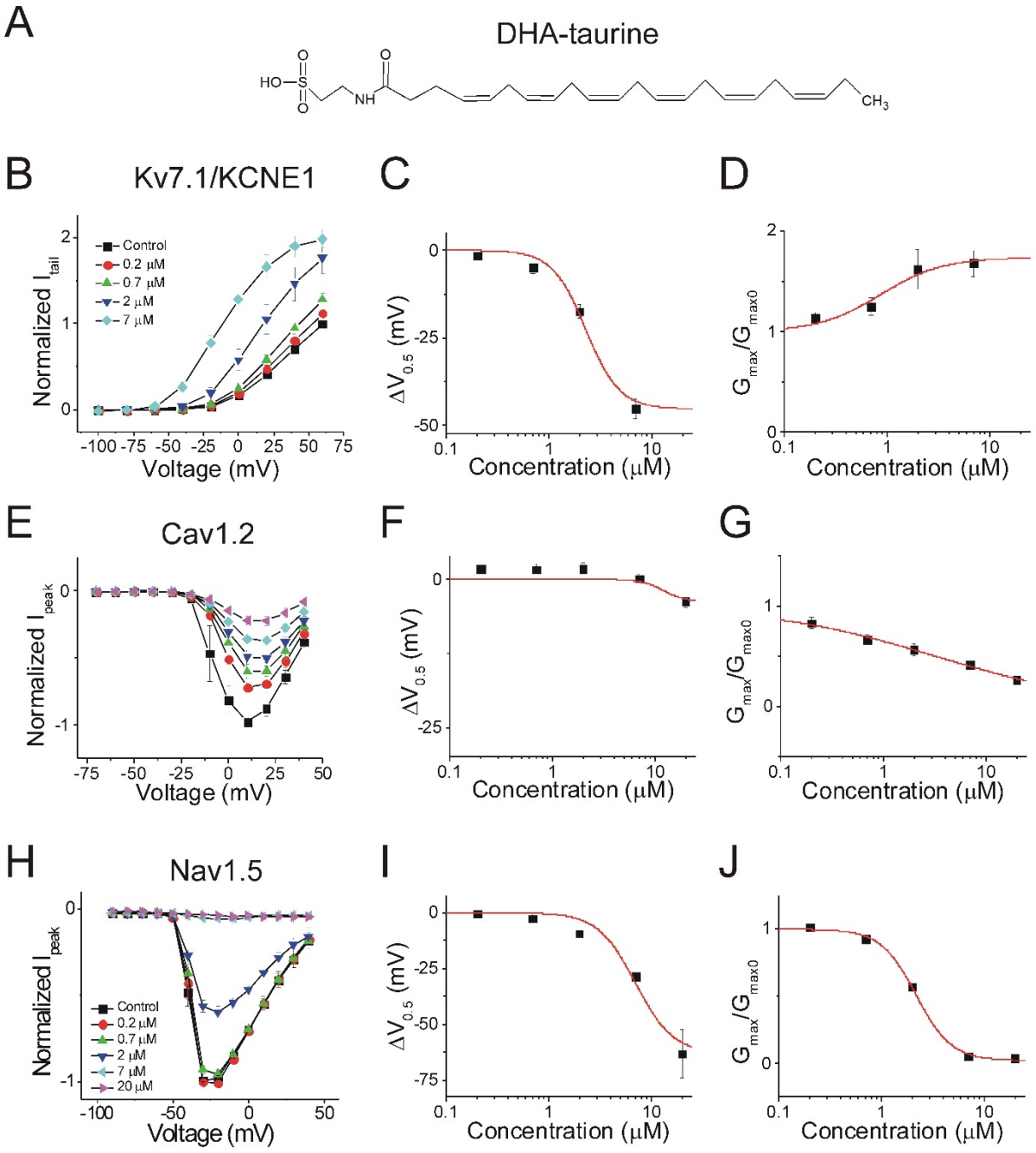

821

822 **Figure 7: Docosahexanoyl-taurine has broad selectivity for Kv7.1/KCNE1, Cav1.2,**
823 **and Nav1.5. A)** Structure of docosahexanoyl taurine (DHA-taurine). **B)** Current-voltage
824 relationship of DHA-taurine on Kv7.1/KCNE1 channels (mean ± SEM; n = 3). **C)** Dose
825 response of the shift in voltage dependent activation ($\Delta V_{0.5}$) of Kv7.1/KCNE1 channels
826 in the presence of DHA-taurine. **D)** Dose response of the change in maximal
827 conductance (G_{max}) of Kv7.1/KCNE1 channels in the presence of DHA-taurine. **E)**
828 Current-voltage relationship of DHA-taurine on Cav1.2 channels (mean ± SEM; n = 3).
829 **F)** Dose response of the shift in voltage dependent inactivation ($\Delta V_{0.5}$) of Cav1.2
830 channels in the presence of DHA-taurine. **G)** Dose response of the change in maximal
831 conductance (G_{max}) of Cav1.2 channels in the presence of DHA-taurine. **H)** Current-
832 voltage relationship of DHA-taurine on Nav1.5 channels (mean ± SEM; n = 3). **I)** Dose
833 response of the shift in voltage dependent inactivation ($\Delta V_{0.5}$) of Nav1.5 channels in the
834 presence of DHA-taurine. **J)** Dose response of the change in maximal conductance
835 (G_{max}) of Nav1.5 channels in the presence of DHA-taurine.

836

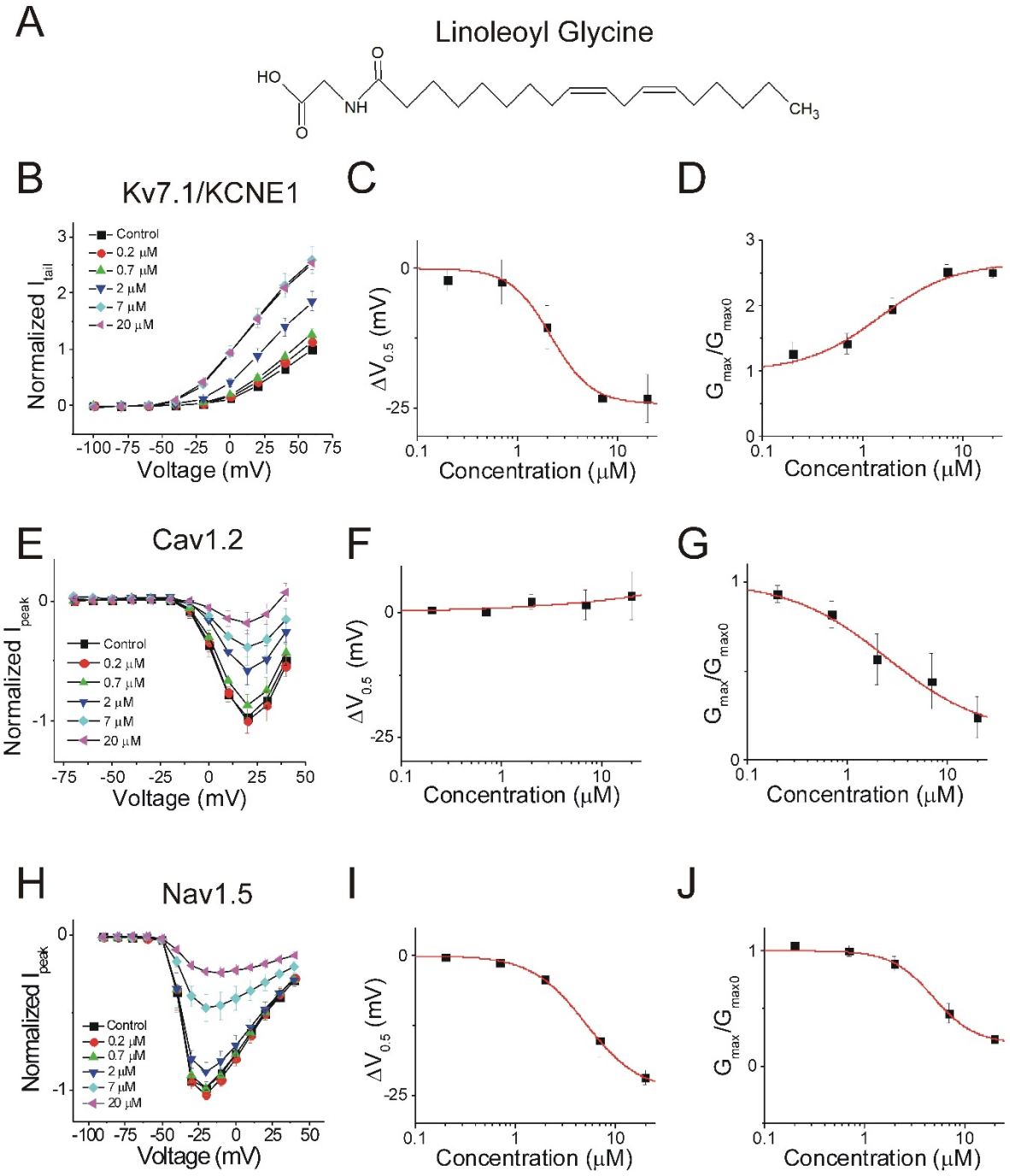

837

838 **Figure 8: Linoleoyl glycine has broad selectivity for Kv7.1/KCNE1, Cav1.2, and**
839 **Nav1.5. A)** Structure of Linoleoyl glycine (Lin-glycine). **B)** Current-voltage relationship of
840 lin-glycine on Kv7.1/KCNE1 channels (mean ± SEM; n = 4). **C)** Dose response of the
841 shift in voltage dependent activation ($\Delta V_{0.5}$) of Kv7.1/KCNE1 channels in the presence
842 of lin-glycine. **D)** Dose response of the change in maximal conductance (G_{max}) of
843 Kv7.1/KCNE1 channels in the presence of Lin-glycine. **E)** Current-voltage relationship of
844 lin-glycine on Cav1.2 channels (mean ± SEM; n = 4). **F)** Dose response of the shift in
845 voltage dependent inactivation ($\Delta V_{0.5}$) of Cav1.2 channels in the presence of lin-glycine.
846 **G)** Dose response of the change in maximal conductance (G_{max}) of Cav1.2 channels in
847 the presence of lin-glycine. **H)** Current-voltage relationship of Lin-glycine on Nav1.5
848 channels (mean ± SEM; n = 4). **I)** Dose response of the shift in voltage dependent
849 inactivation ($\Delta V_{0.5}$) of Nav1.5 channels in the presence of lin-glycine. **J)** Dose response
850 of the change in maximal conductance (G_{max}) of Nav1.5 channels in the presence of lin-
851 glycine.

852

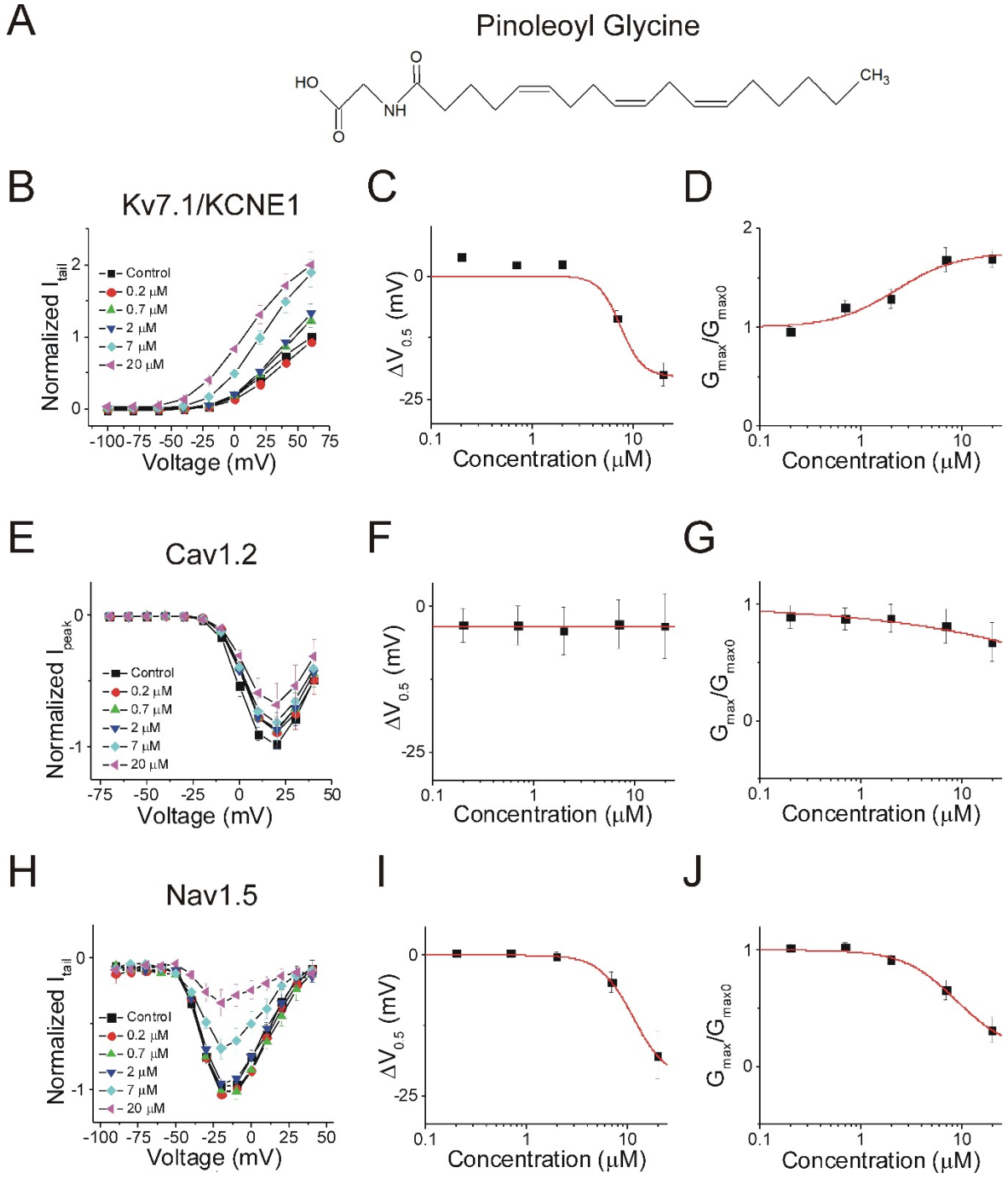

853

Figure 9: Pinoleoyl glycine is more selective for Kv7.1/KCNE1 and Nav1.5 channels than for Cav1.2. A) Structure of Pinoleoyl glycine (Pin-glycine). **B)** Current-voltage relationship of pin-glycine on Kv7.1/KCNE1 channels (mean ± SEM; n = 3). **C)** Dose response of the shift in voltage dependent activation ($\Delta V_{0.5}$) of Kv7.1/KCNE1 channels in the presence of pin-glycine. **D)** Dose response of the change in maximal conductance (G_{max}) of Kv7.1/KCNE1 channels in the presence of Pin-glycine. **E)** Current-voltage relationship of pin-glycine on Cav1.2 channels (mean ± SEM; n = 3). **F)** Dose response of the shift in voltage dependent inactivation ($\Delta V_{0.5}$) of Cav1.2 channels in the presence of pin-glycine. **G)** Dose response of the change in maximal conductance (G_{max}) of Cav1.2 channels in the presence of Pin-glycine. **H)** Current-voltage relationship of pin-glycine on Nav1.5 channels (mean ± SEM; n = 4). **I)** Dose response of the shift in voltage dependent inactivation ($\Delta V_{0.5}$) of Nav1.5 channels in the presence of pin-glycine. **J)** Dose response of the change in maximal conductance (G_{max}) of Nav1.5 channels in the presence of pin-glycine.

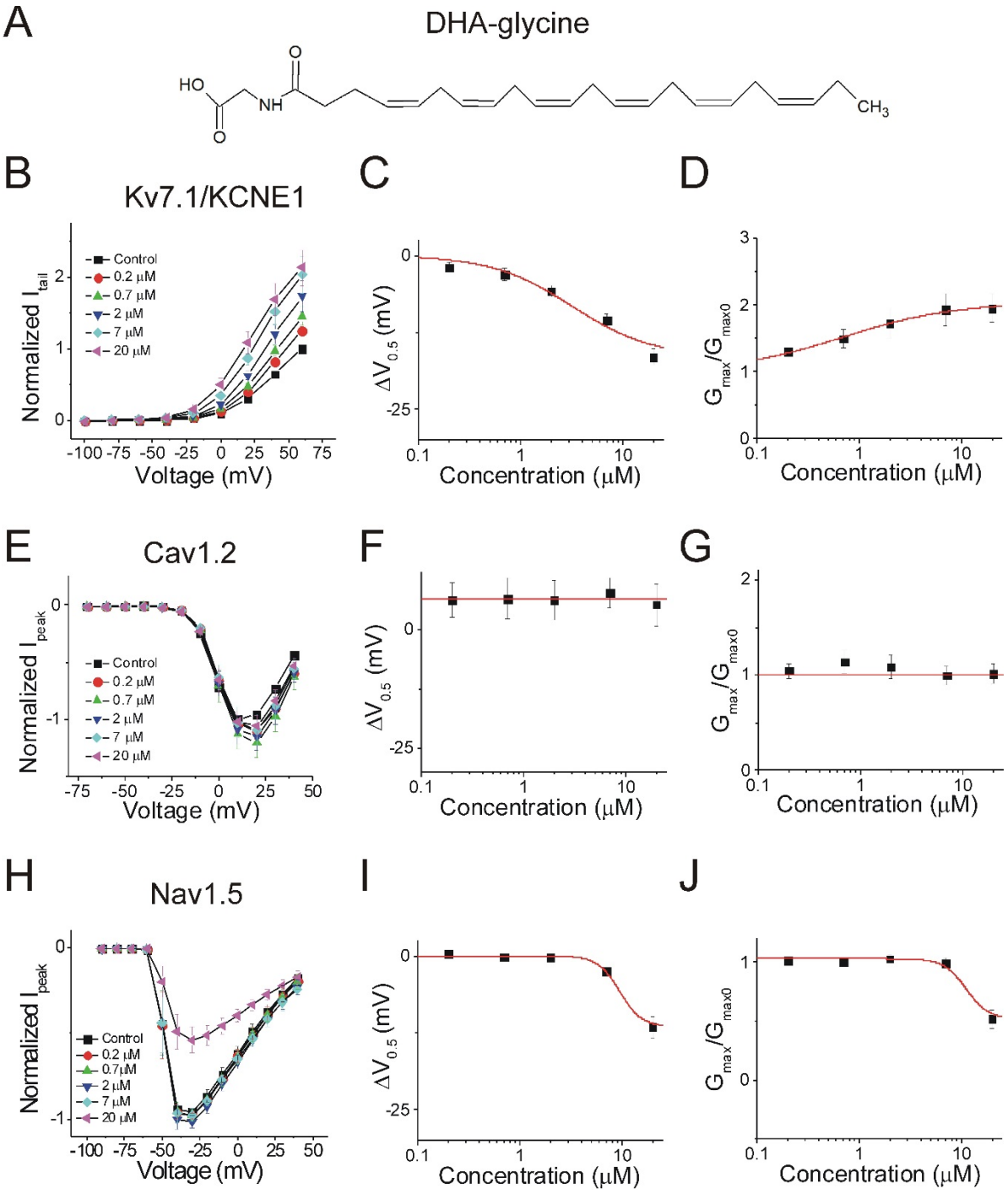

869

Figure 10: Docosahexanoyl glycine is more selective for Kv7.1/KCNE1 channels. **A)** Structure of docosahexanoyl glycine (DHA-glycine). **B)** Current-voltage relationship of DHA-glycine on Kv7.1/KCNE1 channels (mean ± SEM; n = 4). **C)** Dose response of the shift in voltage dependent activation ($\Delta V_{0.5}$) of Kv7.1/KCNE1 channels in the presence of DHA-glycine. **D)** Dose response of the change in maximal conductance (G_{max}) of Kv7.1/KCNE1 channels in the presence of DHA-glycine. **E)** Current-voltage relationship of DHA-glycine on Cav1.2 channels (mean ± SEM; n = 3). **F)** Dose response of the shift in voltage dependent inactivation ($\Delta V_{0.5}$) of Cav1.2 channels in the presence of DHA-glycine. **G)** Dose response of the change in maximal conductance (G_{max}) of Cav1.2 channels in the presence of DHA-glycine. **H)** Current-voltage relationship of DHA-glycine on Nav1.5 channels (mean ± SEM; n = 7). **I)** Dose response of the shift in voltage dependent inactivation ($\Delta V_{0.5}$) of Nav1.5 channels in the presence of DHA-glycine. **J)** Dose response of the change in maximal conductance (G_{max}) of Nav1.5 channels in the presence of DHA-glycine.

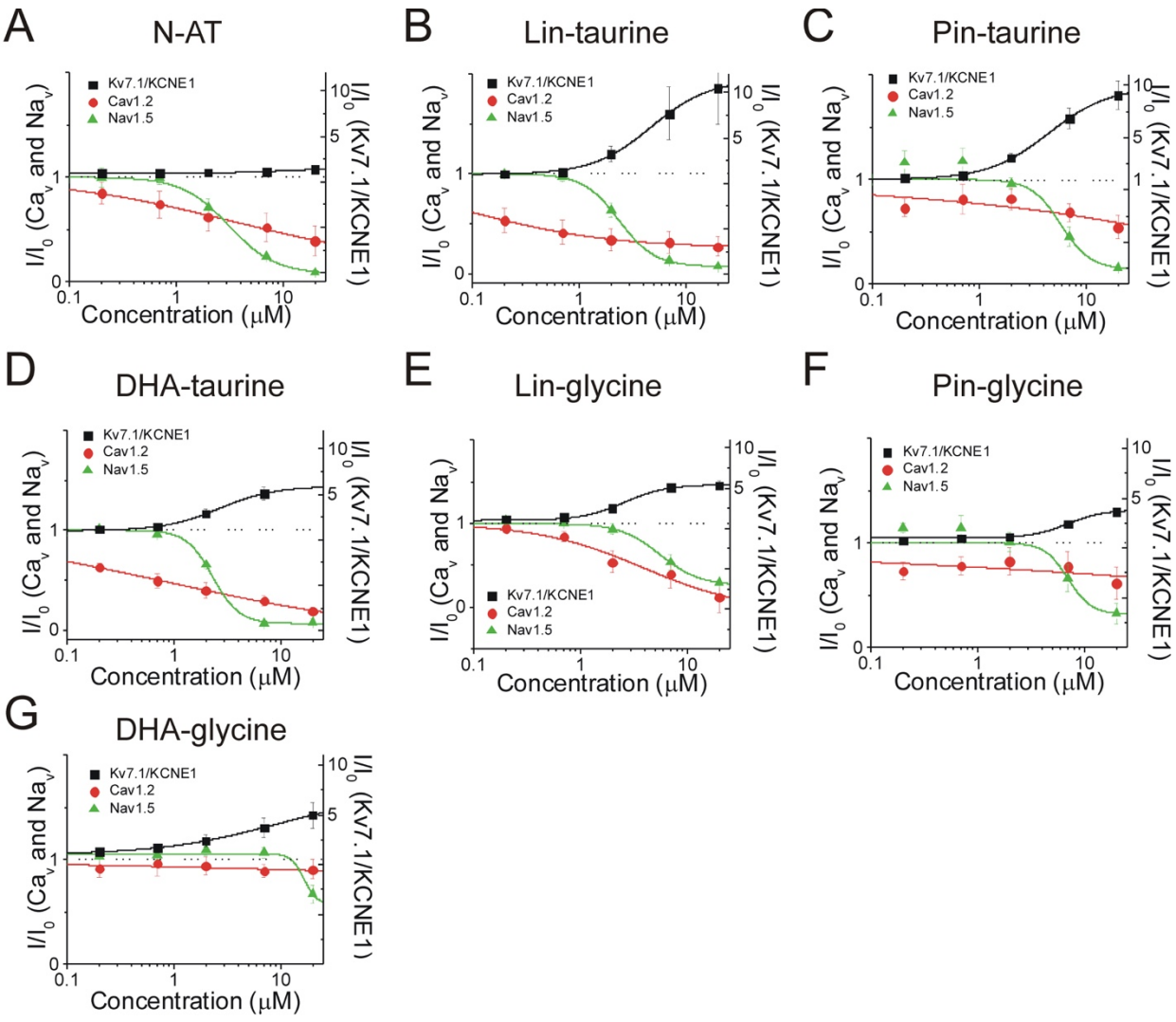

885

886 **Figure 11: Dose response curves for PUFAs on I_{Ks}, I_{CaL}, and I_{NaV} at 0 mV.** Dose
887 response of **A)** N-AT, **B)** lin-taurine, **C)** pin-taurine, **D)** DHA-taurine, **E)** lin-glycine, **F)**
888 pin-glycine, and **G)** DHA-glycine on I_{Ks}, I_{CaL}, and I_{NaV} currents (I/I_0) at 0 mV.

889

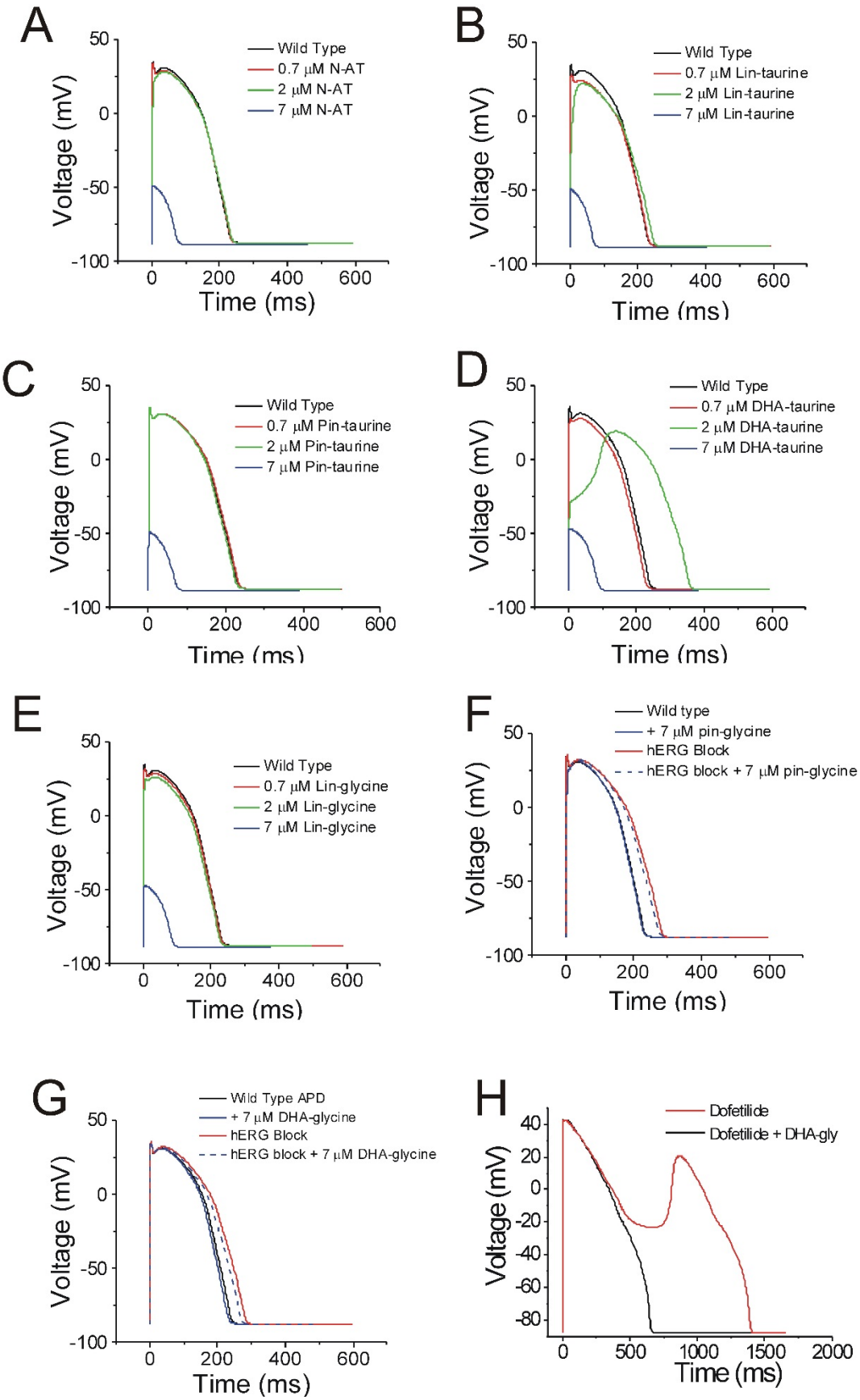

890

Figure 12: PUFAs that are selective for Kv7.1/KCNE1 channels partially restore prolonged ventricular action potential and suppress early afterdepolarizations. A-G) Simulated ventricular action potential in wild type cardiomyocytes (black) and in the presence of **A)** 0.7 (red), 2 (green), and 7 μM N-AT (blue), **B)** 0.7 (red), 2 (green), and 7 μM lin-taurine (blue), **C)** 0.7 (red), 2 (green), and 7 μM pin-taurine (blue), **D)** 0.7 (red), 2 (green), and 7 μM DHA-taurine (blue), **E)** 0.7 (red), 2 (green), and 7 μM lin-glycine (blue), **F)** 7 μM pin-glycine (blue solid), following 25% hERG block (red) and in the presence of 7 μM pin-glycine under 25% hERG block (blue dashed), and **G)** 7 μM DHA-glycine (blue solid), following 25% hERG block (red) and in the presence of 7 μM DHA-glycine under 25% hERG block (blue dashed). **H)** Early afterdepolarizations induced by dofetilide application (red) and suppression of early afterdepolarizations by 7 μM DHA-glycine in the presence of dofetilide (black).

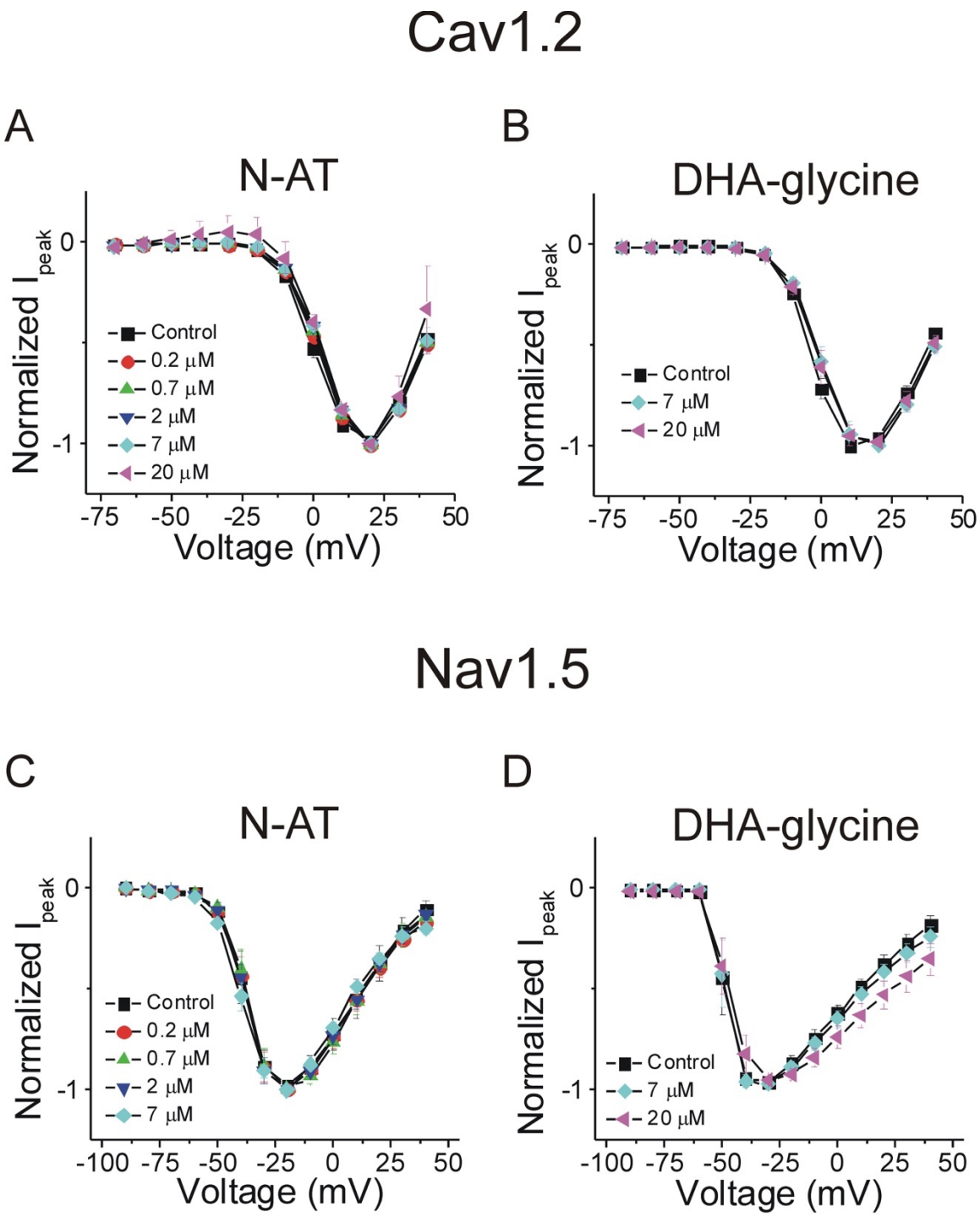

904

Supplemental Figure 1: PUFA-induced changes in I/I_0 normalized by concentration show no changes in voltage-dependent activation of Cav1.2 and Nav1.5 channels. A-B) Voltage-dependent activation of Cav1.2 in the presence of **A)** N-AT and **B)** DHA-glycine. Peak currents are normalized to each concentration to clearly visualize that there is no shifts in voltage-dependent activation. **C-D)** Voltage-dependent activation of Nav1.5 in the presence of **C)** N-AT and **D)** DHA-glycine. Peak currents are normalized to each concentration to clearly visualize that there are no shifts in voltage-dependent activation.